



# Influence of network bond percolation on the thermal, mechanical, electrical and optical properties of high and low- $k$ a-SiC:H thin films



Sean W. King<sup>a,\*</sup>, Jeff Bielefeld<sup>a</sup>, Guanghai Xu<sup>a</sup>, William A. Lanford<sup>b</sup>, Yusuke Matsuda<sup>c</sup>, Reinhold H. Dauskardt<sup>c</sup>, Namjun Kim<sup>d</sup>, Donald Hondongwa<sup>e</sup>, Lauren Olasov<sup>e</sup>, Brian Daly<sup>e</sup>, Gheorghe Stan<sup>f,g</sup>, Ming Liu<sup>h,i</sup>, Dhanadeep Dutta<sup>h,j</sup>, David Gidley<sup>h</sup>

<sup>a</sup> Logic Technology Development, Intel Corporation, Hillsboro OR 97124, USA

<sup>b</sup> Department of Physics, University at Albany, Albany NY 12222, USA

<sup>c</sup> Department of Materials Science and Engineering, Stanford University, Stanford CA 94305, USA

<sup>d</sup> Department of Geological and Environmental Sciences, Stanford University, Stanford CA 94305, USA

<sup>e</sup> Department of Physics and Astronomy, Vassar College, Poughkeepsie NY 12604, USA

<sup>f</sup> Material Measurement Laboratory, National Institute of Standards and Technology, Gaithersburg MD 20899, USA

<sup>g</sup> Department of Mechanical Engineering, University of Maryland, College Park, MD 20742, USA

<sup>h</sup> Department of Physics, University of Michigan, Ann Arbor MI 48109, USA

<sup>i</sup> Nuclear Reactor Program, Department of Nuclear Engineering, North Carolina State University, Raleigh NC 27695, USA

<sup>j</sup> Radiochemistry Division, Bhabha Atomic Research Center, Trombay, Mumbai 400 085 India

## ARTICLE INFO

### Article history:

Received 1 July 2013

Available online 25 August 2013

### Keywords:

Silicon carbide;

Bond percolation;

Constraint theory;

Low- $k$ ;

Plasma;

Chemical vapor deposition

## ABSTRACT

As demand for lower power and higher performance nano-electronic products increases, the semiconductor industry must adopt insulating materials with progressively lower dielectric constants (i.e. low- $k$ ) in order to minimize capacitive related power losses in integrated circuits. However in addition to a lower dielectric constant, low- $k$  materials typically exhibit many other reduced material properties that have limited the ability of the semiconductor industry to implement them. In this article, we demonstrate that the reduced material properties exhibited by low- $k$  materials can be understood based on bond constraint and percolation theory. Using a-SiC:H as a case study material, we utilize nuclear reaction analysis, Rutherford backscattering, nuclear magnetic resonance and transmission Fourier transform infra-red spectroscopy measurements to determine the average coordination ( $\langle r \rangle$ ) for these materials. Correlations of  $\langle r \rangle$  to Young's modulus, hardness, thermal conductivity, resistivity, refractive index, intrinsic stress, mass density and porosity show that an extremely wide range in material properties (in some cases several orders of magnitude) can be achieved through reducing  $\langle r \rangle$  via the controlled incorporation of terminal Si-H<sub>x</sub> and C-H<sub>x</sub> groups. We also demonstrate that the critical point at  $\langle r \rangle \leq 2.4$  predicted by constraint theory exists in this material system and places limitations on the range of properties that can be achieved for future low- $k$  a-SiC:H materials.

© 2013 Elsevier B.V. All rights reserved.

## 1. Introduction

Materials with low dielectric constants (i.e. low- $k$ ) are becoming increasingly important to the semiconductor micro/nano-electronics industry as it strives to maintain Moore's law [1,2]. Low- $k$  materials were initially of primary importance for replacing SiO<sub>2</sub> as the interlayer dielectric (ILD) in metal interconnect structures as a means to reduce parasitic capacitive power losses and resistance-capacitance (RC) delays [3]. However, low- $k$  materials are also needed to replace the relatively higher  $k$  a-SiN:H etch stop, Cu capping, and passivation layers utilized in metal interconnects [4–6]. At the transistor level, there is also

a strong motivation to employ low- $k$  materials in order to reduce parasitic capacitances resulting from trench isolation and sidewall spacer materials that have relatively high values of dielectric constant [7].

Unfortunately, low- $k$  dielectric materials in addition to exhibiting reduced dielectric constants also exhibit reduced values for many other important material properties including Young's modulus [1,2,8–10], fracture toughness [9,10], breakdown field [11,12], thermal conductivity [13,14], and thermal stability [15]. This combined with the introduction of nano-porosity to achieve ultra low- $k$  materials ( $k < 2.5$ ) has made the implementation of low- $k$  materials in micro/nano-electronic products extremely challenging [16,17]. These difficulties have caused the roadmap for the introduction of increasingly lower- $k$  ILD materials forecasted by the International Technology Roadmap for Semiconductors (ITRS) to be pushed out numerous times [18]. It has also caused some corporations to consider more exotic and expensive

\* Corresponding author. Tel.: +1 503 613 7547; fax: +1 971 214 7811.

E-mail address: [sean.king@intel.com](mailto:sean.king@intel.com) (S.W. King).

low- $k$  alternatives such as selective air gap formation [19] and pore-stuffing [20]. For these reasons, a greater understanding of the interplay between the structure and properties of low- $k$  materials is needed.

In this regard, many of the phenomena observed with low- $k$  materials can likely be understood through constraint and bond percolation theory [21–26]. Constraint theory for two and three dimensionally networked materials basically considers the number of degrees of translational freedom and bond constraints (average coordination –  $\langle r \rangle$ ) for each atom and seeks to predict observed material properties for a network of these atoms [27–35]. One interesting aspect of constraint theory is the existence of a critical point or singularity where the number of degrees of freedom equals the number of constraints [21–26,36,37]. For materials where the number of constraints is less than the available degrees of freedom, the system is under constrained and considered “floppy” or “deformable” [38–40]. Conversely, if the number of constraints is greater than the number of degrees of freedom, the system is over constrained and considered “rigid” [38,39]. More importantly, many of the material properties for under constrained systems are predicted to be invariant with  $\langle r \rangle$ , while the material properties for over constrained systems are predicted to increase with increasing  $\langle r \rangle$  [27–30]. The latter is essentially the result of network bonding (rigidity) percolating through the system and in this regard is also sometimes referred to as scaling theory [33,34].

Constraint theory and bond percolation concepts are directly applicable to the material property challenges of low- $k$  dielectrics. Typical low- $k$  materials are inorganic–organic SiO<sub>2</sub> or SiC network materials that are made “low- $k$ ” via the intentional incorporation of terminal hydrogen and organic groups (typically methyl – CH<sub>3</sub>) [1,2]. The terminal groups disrupt the network bonding and create free volume or “porosity” in the material [41,42]. As the dielectric constant of the free volume is by definition equal to one, this results in a reduction in the effective dielectric constant of the material via volume averaging of the  $k$  of the atomic network and the free volume/porosity. However, this also effectively reduces the average network bonding (or connectivity =  $\langle r \rangle_{\text{net}}$ ) of the material leading to a reduction in material properties such as Young’s modulus, hardness, and thermal conductivity [8–15,43,44].

Early in the development of constraint theory for covalently bonded materials, it was predicted that optimum glass forming materials would have compositions at or near the constraint critical point. Since then, constraint theory has been applied to the study of numerous oxide [21,45–47], chalcogenide [48–54], and metallic glasses [55] with great success. However, constraint theory has been applied to the investigation of low- $k$  materials in only a few cases [56–59]. These studies have focused on interpreting the trends in mechanical properties observed for organic–inorganic a-SiOC:H materials of interest for replacing SiO<sub>2</sub> as the ILD material in Cu interconnect structures [1,2]. In the present study, we have chosen low- $k$  amorphous hydrogenated silicon carbide (a-SiC:H) as a case study material for investigating the role of constraint theory and network bond percolation on the thermal, mechanical, electrical, and optical properties of low- $k$  materials. While carbon rich a-SiC:H (polycarbosilanes) films have been previously considered for low- $k$  ILD applications [60,61], higher density a-SiC:H and related a-SiCN:H materials are also of interest as potential replacements for a-SiN<sub>x</sub>:H as low- $k$  Cu capping, etch stop, and hard mask layers [62–68]. For these applications, it is also important to achieve the lowest possible dielectric constant while maintaining acceptable thermal, mechanical, electrical, and etch selectivity properties.

It is also important to note that due to good oxidation resistance, biocompatibility, high elastic modulus and other excellent properties, a-SiC:H and a-SiC are of interest as membrane/cantilever materials in micro/nanoelectromechanical (MEM/NEM) device applications [69], X-ray membrane materials [70], protective coatings for biocompatible implants [71], and membranes for microfluidic devices [72]. The wide band gap (2–3 eV) of a-SiC and a-SiC:H also makes the material of interest as an amorphous semiconductor in microelectronic [73], optoelectronic [74], and solar/photovoltaic applications [75]. In addition, a-SiC

and a-SiC:H offer the added flexibility of being able to tune the physical properties of these materials via adjusting the Si/C stoichiometry and/or the hydrogen content. The former allows the realization of materials with properties spanning those of a-Si and a-C [76]. For the latter, we will demonstrate here that controlled hydrogen incorporation allows the preparation of a-SiC:H materials with a still wider range of properties that can be readily explained using constraint and bond percolation theory.

The method by which  $\langle r \rangle$  is manipulated in a-SiC:H also represents an interesting contrast to other constraint theory and percolation studies of silicate and chalcogenide glasses where the average coordination number has been primarily manipulated by controlling the concentration of two, three, and four fold bond forming constituents. For a-SiC:H and other traditional low- $k$  materials, coordination is manipulated instead by inserting one fold terminal hydrogen and organic (CH<sub>x</sub>) groups. In this regard, H and CH<sub>3</sub> can be viewed as a “network modifier” in the same way as Na<sup>+</sup> and halides are respectively viewed as network modifiers in silicate [21,47] and chalcogenide glasses [52].

In this study, we utilize nuclear reaction analysis (NRA), Rutherford backscattering (RBS), nuclear magnetic resonance (NMR), and transmission Fourier transform infra-red (FTIR) spectroscopy, to determine  $\langle r \rangle$  and  $\langle r \rangle_{\text{net}}$  in low- $k$  a-SiC:H materials deposited by plasma enhanced chemical vapor deposition (PECVD). We produce a range of average network coordination numbers via manipulating the PECVD deposition conditions to produce a-SiC:H materials with a range of hydrogen content and C/Si stoichiometry. We correlate  $\langle r \rangle$  to the a-SiC:H thermal, mechanical, electrical, and optical properties determined by a host of techniques including nano-indentation (NI), picosecond laser ultrasonics (PLU), time domain thermoreflectance (TDTR), spectroscopic ellipsometry (SE), X-ray reflectivity (XRR), ellipsometric porosimetry (EP), positronium annihilation lifetime spectroscopy (PALS) and Hg probe capacitance–voltage (CV) and current–voltage (IV) measurements. We demonstrate that the observed trends in material properties with hydrogen content can be easily understood using bond percolation/constraint theory. We also demonstrate the existence of the critical inflection point at  $\langle r \rangle \leq 2.4$  predicted by constraint theory. Some experimental evidence of a critical average coordination number has been previously reported for a variety chalcogenide glass compositions [39–41,48–53] and discussed in some investigations of a-Si:H [77,78] a-C:H [79–81], and a-CF<sub>x</sub> materials [82,83]. However in these studies, the focus has been primarily on bond/rigidity percolation and, to the author’s knowledge, the presence of a critical point in pure group IV materials has yet to be clearly demonstrated experimentally. Knowledge of a critical coordination number in a-SiC:H could prove useful in further exploiting and refining the numerous properties available from SiC based materials. Lastly, we discuss the implications that constraint theory places on the range of properties achievable for generic inorganic–organic low- $k$  materials.

## 2. Experimental

### 2.1. Film deposition

The details of the films and deposition methods utilized in this study have been previously described in detail [42–44,84,85]. Briefly, all a-SiC:H films were deposited using standard commercially available parallel plate capacitance PECVD tools. The films were deposited on double side polished 300 mm diameter (100) Si substrates using various silane and methylsilane like sources diluted in gases such as H<sub>2</sub> or He. Most films were deposited at temperatures on the order of 400 °C, however, some lower density films were deposited at temperatures on the order of 250 °C. For the lowest density film, a sacrificial organic porogen was intentionally added to the deposition process to facilitate the creation of significant levels of interconnected nano-pores in the a-SiC:H film. In this case, the porogen was removed after deposition using an industry standard electron beam cure [86]. The density/hydrogen content of

the deposited films was further controlled by methods similar to those described by others [8,64,87], which included adjusting the deposition temperature and pressure, reactant/diluent ratio, and the amount of applied high (13.56 MHz) and low (200–400 kHz) frequency power to the plasma. To investigate a fully networked, 0% hydrogen SiC film, an additional sample of single crystal 3C–SiC was obtained from the research group of Prof. Saddow at the University of South Florida. This sample consisted of a 500 nm thick 3C–SiC epilayer heteroepitaxially grown by CVD on a single-side polished 50 mm diameter [100] Si substrate [88].

## 2.2. Film characterization

The details of the FTIR, NRA–RBS, NMR, PLU, TDTR, NI, SE, Hg Probe, XRR, EP, and PALS measurements have all been previously described in detail and will briefly be mentioned here [8,42–44,89–109]. The concentrations of all elements in the a-SiC:H films were determined by elastic scattering and nuclear reaction methods using the Albany Dynamitron Accelerator Laboratory [90]. The H analysis was performed using the  $^{15}\text{N}$  nuclear reaction method. This method makes use of a resonant nuclear reaction between  $^{15}\text{N}$  and H in the target material. By measuring the number of characteristic gamma-rays from this reaction versus beam energy, the H concentration versus depth in the target is determined. The C and O contents were determined using deuteron nuclear reactions. The samples were bombarded with a deuteron beam at 1.2 MeV and the  $^{12}\text{C}(\text{d},\text{p}_0)$  and  $^{16}\text{O}(\text{d},\text{p}_0)$  nuclear reactions were used to determine the C and O contents of the film (in atoms/cm $^2$ ) [91]. 2 MeV  $^4\text{He}$  Rutherford backscattering spectrometry (RBS) was used to determine the Si contents [92]. With the film's absolute H, C, O, and Si compositions, parameter free simulations of the full RBS spectra were performed using the program RUMP [93]. These RUMP simulations were then compared to the data providing a powerful check that the film analysis was correct.

Since carbon may exist in a-SiC:H with both three ( $\text{sp}^2$ ) and four ( $\text{sp}^3$ ) fold coordination,  $^{13}\text{C}$  and  $^{29}\text{Si}$  magic angle spinning (MAS) NMR spectroscopy was performed. Powder samples (typically about 20–25 mg) were prepared for NMR characterization by removing the a-SiC:H films from the silicon substrates with a razor blade. The spectra were collected using a Varian Infinity Plus 400 spectrometer (9.4 T) at 100.52 MHz for  $^{13}\text{C}$  and 79.42 MHz for  $^{29}\text{Si}$ . A 3.2 mm Varian/Chemagnetics T3 MAS probe was used with spinning rates of 12 kHz [96]. Spectra were collected with single pulse acquisition without cross polarization, to ensure quantitative peak areas. For  $^{13}\text{C}$ , a pulse length of 1.2  $\mu\text{s}$  (45° RF tip angle) and a pulse delay of 60 s were used to ensure that measured relative peak intensities were not affected by differential relaxation. A spectrum was also collected with a 360 s pulse delay for one sample and no significant intensity increase was observed. Chemical shifts were referenced to tetramethylsilane (TMS) at 0 ppm for both  $^{13}\text{C}$  and  $^{29}\text{Si}$  [97]. The  $^{13}\text{C}$  NMR data was specifically utilized to differentiate hybridization of C atoms in the a-SiC:H films. The percentage of  $\text{sp}^2$  to  $\text{sp}^3$  C atoms was determined by taking the ratio of the area under the peaks corresponding to the two configurations [98].

The average coordination or connectivity  $\langle r \rangle$  for the a-SiC:H films was calculated using the NRA–RBS and NMR data according to the following expression:

$$\langle r \rangle = \frac{(4[\text{Si}] + 4[\text{C}] \times \% \text{sp}^3 + 3[\text{C}] \times \% \text{sp}^2 + 2[\text{O}] + [\text{H}])}{([\text{Si}] + [\text{C}] + [\text{O}] + [\text{H}])} \quad (1)$$

where [Si], [C], [O], and [H] signify the atomic concentration of Si, C, O, and H in the a-SiC:H films. We have previously estimated the one standard deviation accuracy for the individual atomic concentrations to be  $\pm 5\%$  [94]. Based on this, we believe that the uncertainty in the calculated values for  $\langle r \rangle$  is approximately  $\pm 0.05$ .

FTIR spectra were collected in transmission mode at room temperature using both Nicolet Magna-IR 860 and Bio-Rad QS-3300

spectrometers [8]. Scans were made from 400 to 4000  $\text{cm}^{-1}$  with a resolution of 2  $\text{cm}^{-1}$  and averaged over 64 scans. The intensity of the various relevant absorption bands was determined by integrating the peak area using Win-IR Pro software (ver. 2.5, Bio-Rad Laboratories). More detailed analysis and curve fitting of the various absorption bands were performed utilizing OMNIC software (ver. 8.0, Thermo Fisher Scientific Inc.) [42]. Calibrated cross sections for the terminal  $\text{CH}_x$  and  $\text{SiH}_x$ , network SiC, and impurity  $\text{SiO}$  absorption bands were utilized to calculate the concentrations of [C–H], [Si–H], [Si–C], and [Si–O] bonding in the a-SiC:H materials [94,95]. The concentrations of homopolar C–C and Si–Si bonds ([C–C] and [Si–Si] respectively) were deduced from the combined NRA–RBS and FTIR measurements and mass balance constraints.

Film densities were obtained from both XRR and RBS measurements. The XRR spectra were collected using both a Bede Fab200 Plus (employing a Cu microbeam source and an asymmetric cut Ge crystal), and a Siemens D5000 (employing a Cu line source and graphite monochromator) [99]. The data was collected in the range of 0 to 9000–15,000 arcseconds with approximately 20 arcsecond steps. Spectra were acquired from both 25 and 500 nm a-SiC:H films and fitted using the REFS<sup>TM</sup> software package (version 4.0, Bede). For the 25 nm films, the XRR spectra were fitted by adjusting film thickness, mass density, and surface/interface roughness. For 500 nm films, the thickness was fixed at 500 nm and the spectra fitted by adjusting mass density only. In both cases, excellent fits were obtained and the fitted mass densities agreed to within  $\pm 5\%$ .

Young's modulus and hardness were determined from nano-indentation measurements on 2 micron thick films performed using a Nano XP nanoindenter with a Berkovich diamond tip indenter [99]. Fifteen indents, spaced at 100  $\mu\text{m}$ , were made on each sample using a load range of 5–30 mN. Samples were loaded in continuous stiffness mode. The hardness and modulus were calculated using a contact depth range of 200–400 nm for hardness and 50–150 nm for modulus to avoid substrate interactions. A Poisson's ratio of 0.25 was assumed. Young's modulus for the a-SiC:H films was additionally determined by contact resonance atomic force microscopy (CR-AFM) measurements that have been previously reported [100].

The longitudinal sound velocity  $v_l$  of the a-SiC:H films was measured by PLU [98,99], and the thermal conductivity  $\kappa$  was measured by TDTR [101]. Both techniques require a thin (40–80 nm) film of aluminum to be deposited on top of the thin film of interest. This was accomplished in this study by e-beam evaporation. PLU and TDTR are ultrafast pump-probe measurements, and use short laser pulses (less than 100 fs) from a Ti:sapphire oscillator operating at a repetition rate of 76 MHz. Young's modulus for the a-SiC:H films was determined from the PLU sound velocity measurements using relationships that have been previously described [101]. Similarly, thermal conductivity was determined from the TDTR measurements by monitoring and modeling the temperature dependent change in reflectivity of the Al/a-SiC:H sample as heat dissipated from the Al film into the a-SiC:H dielectric [102].

The low frequency dielectric constant ( $k$ ) of these materials was determined by metal-insulator-semiconductor (MIS) CV measurements using a Hg probe at 100 kHz [103]. Leakage currents/resistivities were determined by separate IV measurements performed using the same Hg Probe system. Film thickness and refractive index were measured using a J. A. Woollam variable angle Spectroscopic Ellipsometer (VASE) [104,105]. Refractive index (RI) values are reported at a wavelength of 673 nm. Intrinsic film stress was calculated using Stoney's formula [106] and the optically determined film thickness and wafer curvature measured using a laser deflection method [99].

The percent porosity and pore interconnectivity for the films investigated were determined by ellipsometric porosimetry [107] using a vacuum system equipped with a separate spectroscopic ellipsometer to measure changes in the optical properties of the porous materials upon exposure to the vapor of various different solvents. The pore size of the a-SiC:H films was additionally examined with positronium

**Table 1**  
Summary of a-SiC:H mass density and atomic composition determined by NRA–RBS measurements and  $^{13}\text{C}$   $\text{sp}^2/\text{sp}^3$  ratio from NMR.

Film	Dielectric constant “k”	NRA–RBS density ( $\text{g}/\text{cm}^3$ )	% C ( $\pm 5\%$ )	% Si ( $\pm 5\%$ )	% O ( $\pm 5\%$ )	% H ( $\pm 5\%$ )	NMR $^{13}\text{C}$ $\text{sp}^2/\text{sp}^3$
3CSiC	9.7	3.21	50	50	0	0	–
SiC:H-14	$7.2 \pm 0.2$	$2.5 \pm 0.1$	36.3	37.1	0.3	26.3	–
SiC:H-13	$6.9 \pm 0.2$	$2.3 \pm 0.1$	34.7	33.9	0.2	31.2	–
SiC:H-12	$6.8 \pm 0.2$	$2.2 \pm 0.1$	34.5	32.4	0.5	32.7	–
SiC:H-11	$6.5 \pm 0.2$	$2.0 \pm 0.1$	33.2	31.5	0.1	35.1	–
SiC:H-10	$6.2 \pm 0.2$	$1.9 \pm 0.1$	31.7	30.8	1.1	36.3	–
SiC:H-9	$5.8 \pm 0.2$	$1.85 \pm 0.1$	29.1	28.2	2.7	40.0	–
SiC:H-8	$5.2 \pm 0.15$	$1.75 \pm 0.1$	27.0	25.1	5.9	41.9	–
SiC:H-7	$4.8 \pm 0.15$	$1.6 \pm 0.1$	28.5	22.2	4.1	45.3	–
SiC:H-6	$4.4 \pm 0.15$	$1.4 \pm 0.1$	24.0	20.5	5.9	49.7	–
SiC:H-5	$4 \pm 0.1$	$1.3 \pm 0.1$	23.1	21.5	9.2	46.1	–
SiC:H-4	$3.7 \pm 0.1$	$1.2 \pm 0.1$	14.8	14.8	12.6	57.8	–
SiC:H-3	$3.6 \pm 0.1$	$1.2 \pm 0.1$	14.8	14.8	12.4	58.0	–
SiC <sub>x</sub> :H-2	$3.2 \pm 0.1$	$1.1 \pm 0.1$	30.2	10.6	9.6	49.6	1.3
SiC <sub>x</sub> :H-1	$2.8 \pm 0.1$	$1.0 \pm 0.1$	30.5	6.0	5.6	57.9	1.5

annihilation lifetime spectroscopy using an electrostatically focused beam of positrons. Details of such beam-PALS measurements have been previously described elsewhere [108,109]. Briefly, PALS spectra with  $\sim 10^7$  events were acquired at room temperature with a channel plate start-fast plastic scintillator stop lifetime system with a time resolution of 500 ps. Positron beam implantation energies from 0.7 to 5.2 keV are used to probe pore interconnectivity and to search for any depth related heterogeneity. None was detected in the films reported herein so PALS results are presented for 3.2 keV beam energy where mean implantation depth is around 100 nm. The fitted average positronium lifetime is related to the average pore diameter,  $D_{\text{sph}}$ , assuming a spherical pore model [108].

### 3. Results and discussion

#### 3.1. NRA–RBS $\langle r \rangle$ and FTIR $\langle r \rangle_{\text{net}}$

In Table 1, we summarize the low frequency dielectric constant, NRA–RBS elemental composition, mass density, and the NMR  $^{13}\text{C}$   $\text{sp}^2/\text{sp}^3$  ratios for the a-SiC:H films investigated in this study. As can be seen,  $k$  ranges from 2.8 to 7.2 and the a-SiC:H films are largely stoichiometric in terms of C/Si ratios. However, the two lowest density films do exhibit significant non-stoichiometry with C/Si ratios of 3–5. It should be noted that these are the only two films for which NMR detected significant levels of  $\text{sp}^2$  related carbon. As would be expected, the dielectric constant and mass density of the a-SiC:H films decrease steadily with increasing hydrogen content. It can also be seen that as hydrogen content increases and mass density decreases, the oxygen content in the films gradually increase. The incorporation of oxygen in the a-SiC:H films is believed to occur after the film deposition and on exposure to ambient conditions. As has been shown previously, moisture permeation through a-SiC:H increases as mass density decreases and becomes quite rapid once interconnected porosity is observed to form [109].

The values of  $\langle r \rangle$  determined by NRA–RBS and NMR for the a-SiC:H films in this study are displayed in Fig. 1 as a function of percent hydrogen. As expected,  $\langle r \rangle$  steadily decreases as hydrogen content increases. At a hydrogen content of  $\sim 50\%$ ,  $\langle r \rangle$  reaches the critical coordination number ( $\langle r \rangle_c$ ) of 2.4 predicted by constraint theory for four fold coordinated group IV materials. However for materials containing one fold coordinated (OFC) atoms,  $\langle r \rangle_c$  is actually a function of the OFC content as has been noted by Boolchand [110]. Specifically for the case of hydrogen as an OFC entity,

$$\langle r \rangle_c^* = 2.4 - 0.4X_{\text{H}}, \quad (2)$$

where  $\langle r \rangle_c^*$  is the OFC modified critical coordination number and  $X_{\text{H}}$  is the fraction or percentage of hydrogen in the system. This OFC modified

critical coordination number is also plotted in Fig. 1 for the a-SiC:H films investigated in this study. As can be seen, the lowest density/highest hydrogen content films fall below both  $\langle r \rangle_c$  and  $\langle r \rangle_c^*$ .

We note that Mousseau et al. [111] have previously predicted that the critical coordination for a-Si $_1 - x\text{Ge}_x\text{H}_y$  alloys and other hydrogenated group four materials should occur at 62 atomic percent hydrogen. Hydrogen contents exceeding this value were not achieved for any of the films in this study. However in the Mousseau calculations, each Si or Ge atom was limited to having no more than two hydrogen bonds to prevent formation of terminal SiH $_3$  or GeH $_3$  species. Mousseau also did not consider the presence of any other intermediate coordination atoms. In our case, the highest hydrogen content films contain an abundance of terminal CH $_3$  groups and also include some lower coordination oxygen impurities from environmental exposure [93]. These two considerations result in  $\langle r \rangle_c^*$  being achieved at hydrogen contents lower than predicted by Mousseau.

To facilitate a better understanding of the local structural changes occurring as hydrogen content increases and  $\langle r \rangle$  decreases, additional quantitative FTIR measurements were performed to determine the concentration of all the significant chemical bonds in the a-SiC:H films [94,95]. In Fig. 2, we display as a function of  $\langle r \rangle$  the ratio of Si–C, Si–H, Si–O, and Si–Si bond densities to the Si atomic density determined by FTIR. Fig. 3 displays similar information for carbon containing bonds (C–Si, C–H, and C–C) normalized by the C atomic density. As can be seen, Si–C bonding represents the largest proportion of network bonds in the a-SiC:H materials, but decreases with  $\langle r \rangle$  as hydrogen content increases. This trend continues until  $\langle r \rangle \cong 2.4$  where there is a

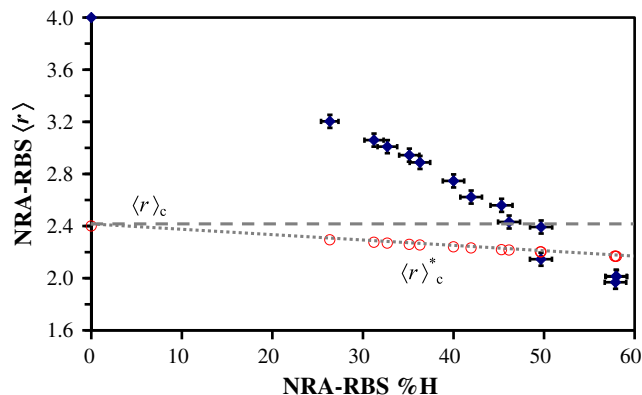


**Fig. 1.** Percent hydrogen (%H) vs. average coordination number ( $\langle r \rangle$ ) determined by NRA–RBS for the a-SiC:H films investigated in this study.

sudden shift in the relative proportion of different bonds that results in homopolar Si–Si and C–C bonds becoming more significant than the heteropolar Si–C bonding. This transition from predominantly Si–C bonding to Si–Si and C–C bonding with increased hydrogenation has been observed previously in free energy modeling by Efstathiadis [112]. In this case, the sudden shift from heteropolar to homopolar bonding was attributed to a thermodynamic instability for Si–C bonding in the presence of hydrogen [112].

Also included in Figs. 2 and 3 is the sum of Si network forming bonds ( $\Sigma\text{Si-Net} = [\text{Si-C}] + [\text{Si-O}] + [\text{Si-Si}]$ ) and C network forming bonds ( $\Sigma\text{C-Net} = [\text{Si-C}] + [\text{C-C}]$ ) normalized by the Si and C atomic density respectively. As shown in Fig. 2,  $\Sigma\text{Si-Net}/[\text{Si}]$  decreases from 4 for single crystal 3C–SiC to 3.2 for a-SiC:H at  $\langle r \rangle \cong 2.6$ –2.9 as the hydrogen and Si–H bond concentration increases. However below  $\langle r \rangle = 2.6$ , the Si–H bond concentration decreases and  $\Sigma\text{Si-Net}/[\text{Si}]$  increases again to 3.6–3.7 while hydrogen content continues to increase. This is in contrast to the behavior shown in Fig. 3 where  $\Sigma\text{C-Net}/[\text{C}]$  is observed to steadily decrease with increasing hydrogen content and decreasing  $\langle r \rangle$ . This behavior is due to the preferential formation of C–H over Si–H bonds as an increasing amount of hydrogen is incorporated into a-SiC:H. As shown in Figs. 2 and 3, the concentration of Si–H bonds decreases while C–H bonds continue to increase as the total hydrogen content increases and  $\langle r \rangle$  decreases below 2.6. The continued preferential incorporation of hydrogen as C–H entities leads to the eventual formation of significant concentrations of terminal Si–CH<sub>3</sub> bonds. These terminal Si–CH<sub>3</sub> bonds are included in the total Si–C bond density presented in Fig. 2 both for initial clarity and due to complications arising from overlap of the IR absorption bands for Si–C network and terminal Si–CH<sub>3</sub> bonds.

To better understand the degree of Si network connectivity, we note that the Si–C and Si–CH<sub>3</sub> IR absorption bands were deconvoluted in a previous study. In Fig. 4, we show the ratio of terminal Si–CH<sub>3</sub> bonds to all Si–C bonds as a function of  $\langle r \rangle$ . As can be seen, the concentration of terminal Si–CH<sub>3</sub> bonds is low for high values of  $\langle r \rangle$ . Starting at  $\langle r \rangle \cong 2.6$ –2.7, however, the concentration of terminal Si–CH<sub>3</sub> bonds increases significantly. At this point, it should be noted that terminal Si–SiH<sub>3</sub> and C–CH<sub>3</sub>, bonds and higher order terminal Si–Si(CH<sub>3</sub>)<sub>3</sub> and C–Si(CH<sub>3</sub>)<sub>3</sub> entities are also likely to be present in the a-SiC:H films to some degree. Unfortunately, it is difficult to directly determine the concentration for many of these large terminal entities due to the low IR absorption cross section of homopolar C–C and Si–Si bonds. However, an indirect estimate of the concentration of terminal entities with homopolar bonds can be gained by a detailed examination of the C–H and Si–H absorption bands. Based on our previous quantitative analysis of the C–H and Si–H absorption bands in these materials [94,95], we also present in Fig. 4 estimates for the concentration of terminal C–CH<sub>3</sub>, Si–SiH<sub>3</sub>, Si–Si(CH<sub>3</sub>)<sub>3</sub>, and C–Si(CH<sub>3</sub>)<sub>3</sub> groups.

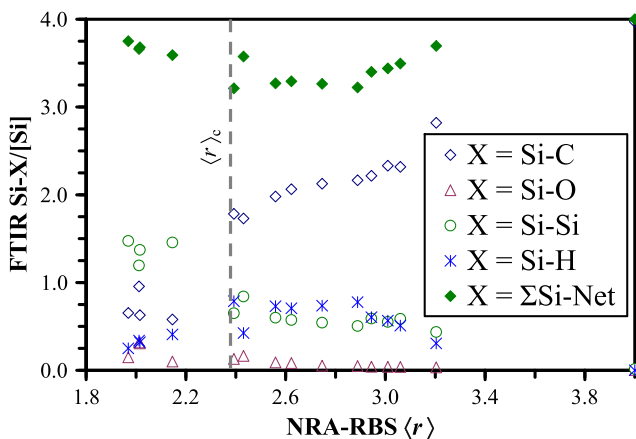


Fig. 2. a-SiC:H FTIR Si bond concentrations (normalized to Si content) vs. NRA-RBS  $\langle r \rangle$ . Note: error bars excluded to more clearly illustrate observed trends.

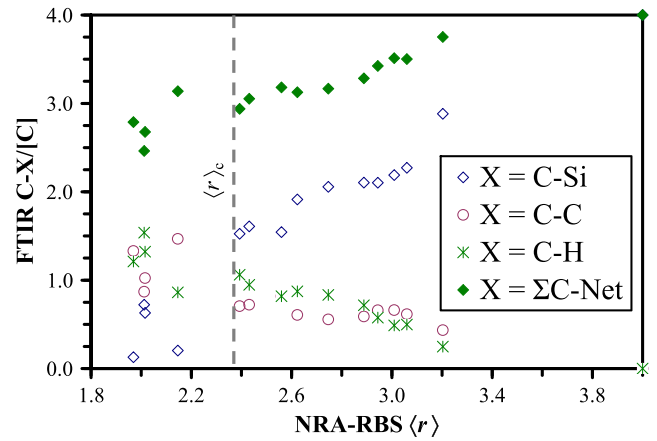


Fig. 3. a-SiC:H FTIR C bond concentrations (normalized to C content) vs. NRA-RBS  $\langle r \rangle$ . Note: error bars excluded to more clearly illustrate observed trends.

After consideration of all the possible terminal bonding modes in the a-SiC:H films, it is now possible to provide an estimate of the individual network connectivity for both the Si and C atoms in a-SiC:H. The average network connectivity of C and Si ( $\langle r \rangle_{\text{C-net}}$  and  $\langle r \rangle_{\text{Si-net}}$  respectively) were estimated based on the FTIR measurements and the following relations:

$$\langle r \rangle_{\text{Si-net}} = (\Sigma[\text{Si-X}]_{\text{All}} - [\text{Si-X}]_{\text{term}}) / [\text{Si}], \quad (3)$$

$$\langle r \rangle_{\text{C-net}} = (\Sigma[\text{C-X}]_{\text{All}} - [\text{C-X}]_{\text{term}}) / [\text{C}], \quad (4)$$

where  $\Sigma[\text{Si-X}]_{\text{All}}$  and  $[\text{Si-X}]_{\text{term}}$  respectively represent the sum of all silicon (or carbon) containing bonds and silicon containing terminal bonds. These estimated values are shown in Fig. 5 where both  $\langle r \rangle_{\text{Si-net}}$  and  $\langle r \rangle_{\text{C-net}}$  are displayed as a function of  $\langle r \rangle$ . As can be seen,  $\langle r \rangle_{\text{Si-net}}$  and  $\langle r \rangle_{\text{C-net}}$  are close to the same for  $\langle r \rangle > 2.4$ . However, at  $\langle r \rangle \sim 2.4$ ,  $\langle r \rangle_{\text{Si-net}}$  and  $\langle r \rangle_{\text{C-net}}$  start to diverge significantly with  $\langle r \rangle_{\text{Si-net}}$  decreasing to 2–2.2 while  $\langle r \rangle_{\text{C-net}}$  ranges from 2 to 2.8. This is an indication that for a-SiC:H films with  $\langle r \rangle < 2.4$ , the C–C bonds are likely the dominant network bonds. Also note that the error bars for  $\langle r \rangle_{\text{SiC}}$  increase from  $\pm 0.05$  for  $\langle r \rangle_{\text{net}} > 2.4$  (not shown for clarity) to 0.1–0.2 for  $\langle r \rangle_{\text{net}} < 2.4$ . These error bars represent a one standard deviation confidence interval and the increased error bars for  $\langle r \rangle_{\text{net}} < 2.4$  is a direct result of additional sources of errors arising due to the complications of distinguishing between the various heteropolar and homopolar networks and terminal bonding modes mentioned above.

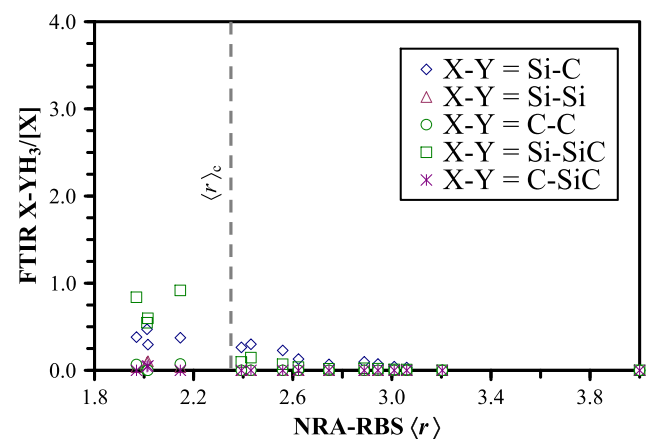


Fig. 4. Estimated a-SiC:H terminal Si–CH<sub>3</sub>, Si–SiH<sub>3</sub>, C–CH<sub>3</sub>, Si–Si(CH<sub>3</sub>)<sub>3</sub>, and C–Si(CH<sub>3</sub>)<sub>3</sub> bond concentrations (normalized to Si content) based on quantitative FTIR measurements.

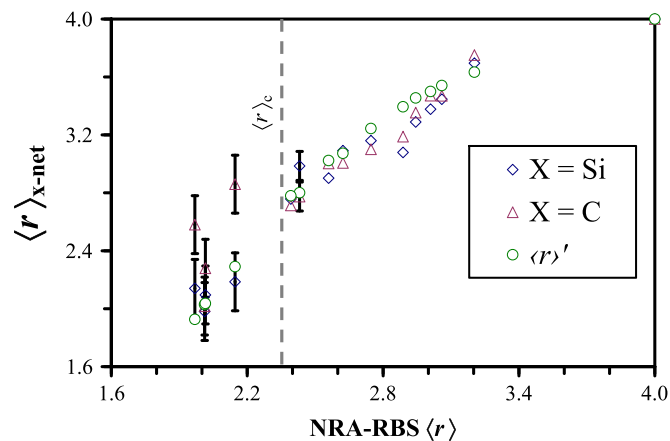


Fig. 5. Estimated a-SiC:H Si and C network connectivity ( $\langle r \rangle_{\text{net}}$ ) and plucked network connectivity ( $\langle r \rangle'$ ) vs. NRA-RBS ( $\langle r \rangle$ ).

Lastly, we note for completeness that for some studies authors have preferred to consider a “plucked” network connectivity ( $\langle r \rangle'$ ) where the contribution of the terminal OFC species are removed or “plucked” from the system [110]. The advantage of considering network connectivity in this fashion is that the critical coordination will in all cases be constant at  $\langle r \rangle_c = 2.4$ . For materials containing OFC species such as hydrogen,  $\langle r \rangle'$  have been shown to be dependent on the hydrogen content according to the relation:

$$\langle r \rangle' = (\langle r \rangle - 2X_{\text{H}}) / (1 - X_{\text{H}}). \quad (5)$$

Unfortunately, this expression does not consider the possibility of terminal  $\text{SiH}_3$ ,  $\text{CH}_3$ ,  $\text{OH}$ , and larger  $\text{Si}(\text{CH}_3)_3$  groups that we have just shown are present in significant quantities for the highest hydrogen content a-SiC:H films investigated in this study. However, factoring these additional terminal entities into the above expression would require the same detailed FTIR analysis we just described. In this case, it is interesting to compare the values of  $\langle r \rangle'$  calculated using Eq. (5) to the values of  $\langle r \rangle_{\text{SiC}}$  previously described. As shown in Fig. 5,  $\langle r \rangle'$  and  $\langle r \rangle_{\text{SiC}}$  generally have similar values for  $\langle r \rangle > 2.4$ . However at  $\langle r \rangle < 2.4$ ,  $\langle r \rangle_{\text{Si}}$  and  $\langle r \rangle_{\text{C}}$  diverge and  $\langle r \rangle'$  interestingly starts to represent the average value of the two.

After having considered several different accounting methods for describing the overall connectivity of the a-SiC:H films described in this study, we will focus on average coordination number  $\langle r \rangle$  going forward. While  $\langle r \rangle_{\text{C,Si}}$  and  $\langle r \rangle'$  may ideally be a more accurate representation of the a-SiC:H network connectivity and allow comparison to a constant critical coordination number, the error bars for these values are substantially larger due to complications in distinguishing between Si–C network bonds and terminal Si–C bonds such as Si– $\text{CH}_3$  and Si– $(\text{CH}_3)_3$ .

### 3.2. Mechanical properties

Fig. 6 displays as a function of  $\langle r \rangle$  the values of Young's Modulus for the a-SiC:H films in this study determined by prior NI, CR-AFM, and PLU measurements [100,102]. As shown, Young's Modulus decreases steadily with decreasing coordination. At  $\langle r \rangle \approx 2.3$ , an inflection point is observed and relatively no change in Young's modulus is detected for further reductions in  $\langle r \rangle$ . This result is consistent with predictions by constraint theory where the elastic constants of group IV, chalcogenide and other materials have been predicted to trend to zero and become invariant with  $\langle r \rangle$  values  $\leq 2.4$ . Fig. 7 displays similar trends for the a-SiC:H hardness determined by nanoindentation measurements. As for Young's modulus, the hardness for the a-SiC:H films was also

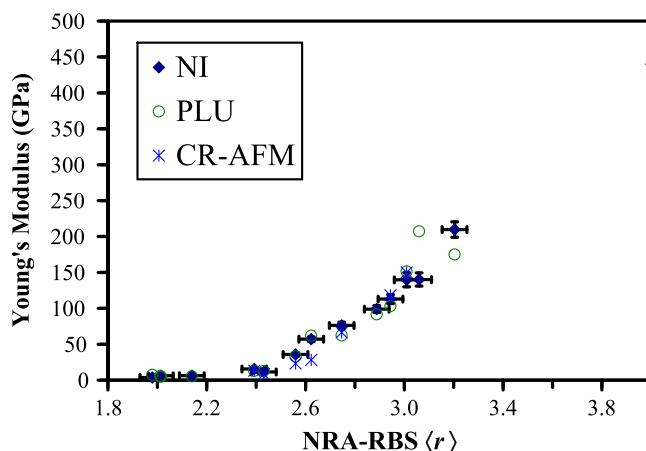


Fig. 6. a-SiC:H Young's modulus as determined by NI, PLU and CR-AFM vs. NRA-RBS ( $\langle r \rangle$ ).

observed to decrease steadily with  $\langle r \rangle$  and become invariant below  $\langle r \rangle$  values of  $\sim 2.3$ .

In addition to a critical coordination number, constraint theory also predicts the elastic constants ( $c_{ij}$ ) of a material should increase with  $\langle r \rangle$  above  $\langle r \rangle_c$  to the power of 1.5 (i.e.  $c_{ij} \propto (\langle r \rangle - \langle r \rangle_c)^{1.5}$ ) [27,30]. To test for this specific exponent dependence, we display in Fig. 8 the nanoindentation Young's modulus ( $E$ ) from Fig. 6 plotted to the  $2/3$  power. As can be seen, a linear relationship between  $E^{2/3}$  and  $\langle r \rangle$  is observed with linear regression analysis indicating an  $R^2$  value of 0.99. A similar linear dependence between hardness $^{2/3}$  and  $\langle r \rangle$  was also observed but with a slightly lower  $R^2$  value of 0.93. In this regard, it is important to note that the depleted network bond analysis by Franzblau has shown that the exact exponent can range from 1.35 to 1.89 and depends on the strength ratio of the bond bending and bond stretching forces [30]. Also the numerical simulations by both He [27] and Franzblau [30] are for an anisotropic crystalline diamond lattice which is in contrast to the amorphous and isotropic a-SiC:H films investigated in this study.

The above results are in contrast to numerous investigations of rigidity percolation in a variety of chalcogenide glass compositions. An early investigation of the  $C_{11}$  and  $C_{44}$  elastic moduli for Ge–As–Se glasses by Halfpap did claim to observe an inflection point at  $\langle r \rangle = 2.4$  [113]. However, several later investigations of the same ternary and other chalcogenide systems have shown a smooth variation in elastic constants and hardness across the predicted critical coordination number [49–51,114–118]. Instead, critical points at  $\langle r \rangle = 1.8$ – $2.0$  [116,118] and  $2.6$ – $2.7$  [132–136] have been observed for the elastic constants and hardness of a variety of binary and ternary chalcogenide glasses.

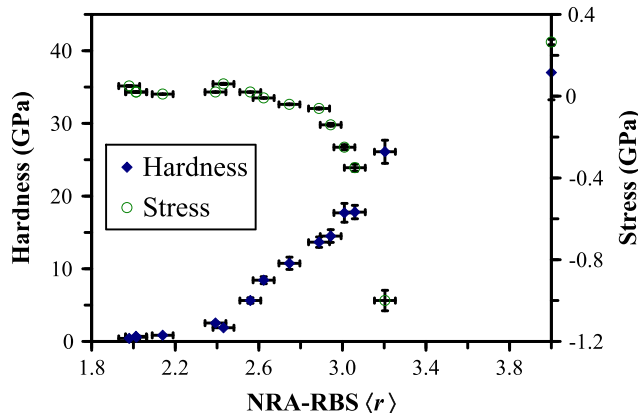


Fig. 7. a-SiC:H nanoindentation hardness and intrinsic film stress vs. NRA-RBS ( $\langle r \rangle$ ).

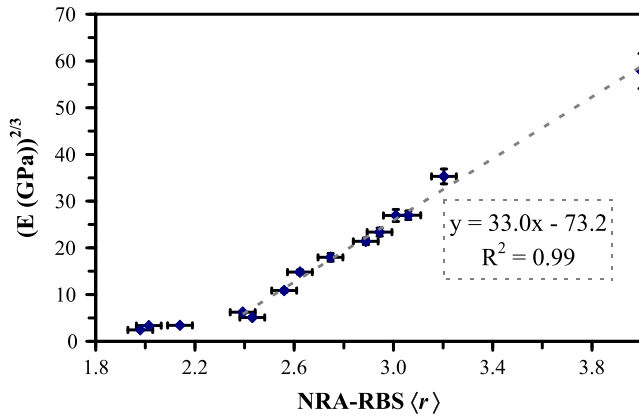


Fig. 8. a-SiC:H (Young's modulus)<sup>2/3</sup> vs. NRA-RBS  $\langle r \rangle$ .

For the former case, Swiler has attributed the singularity at  $\langle r \rangle = 2.0$  to rigidity percolation in 10 atom long Se chains [116]. In the later case, the critical point has been attributed to chemical or medium range ordering effects resulting from achieving the stoichiometric composition of thermodynamic equilibrium chalcogenide compounds [119–123]. As there are no known thermodynamic equilibrium compounds between SiC and H, no critical points are expected at  $\langle r \rangle = 2.6$ –2.7 in the elastic properties of a-SiC:H. However, as we will show later, an inflection point at  $\langle r \rangle = 2.8$  does surprisingly show up in the thermal properties of a-SiC:H films.

The initial results reported by Halfpap have since been attributed by Tatsumisago and others to the unintentional (and initially undetected) presence of oxygen impurities in the Ge–As–Se glasses [115]. For the a-SiC:H films investigated here, oxygen impurities were also observed in the films, particularly as  $\langle r \rangle$  decreases. As stated previously, the oxygen impurities are believed to be due to ambient exposure and ingress diffusion of moisture [109]. In contrast to Halfpap though, the presence and valence of these oxygen impurities are directly factored into our calculation of  $\langle r \rangle$ . Also as oxygen concentrations in the a-SiC:H films are comparable on both immediate sides of  $\langle r \rangle_c$ , we do not believe the oxygen impurities in this case are responsible for the observed inflection point in Young's modulus and hardness.

The lack of an observed inflection point in elastic constants and hardness at the theoretical predicted critical coordination number  $\langle r \rangle_c = 2.4$  for chalcogenides has been attributed to a lack of consideration of so called “weak forces” in the initial analysis. The original simulation by He and Thorpe considered only strong covalent bond stretching and bending forces which unrealistically predicted the elastic constants of a material should go to zero at  $\langle r \rangle < 2.4$  [27]. Later simulations by Cai and Thorpe also included “weak” diangular and inter chain van der Waal type forces [124]. The inclusion of these forces was found to stabilize the lattice and result in more realistic finite elastic constant values for  $\langle r \rangle \leq 2.4$ . More importantly though, these additional forces also resulted in the singularity at  $\langle r \rangle = 2.4$  being completely washed out. However as Cai notes, the appearance of the predicted singularity at  $\langle r \rangle < 2.4$  is directly related to the strength of the “weak forces” considered. Therefore, it is possible the absolute or relative strength of these weak forces in a-SiC:H is reduced in comparison to chalcogenide glasses. In this regard, we note that Cai selected a bond bending ( $\beta$ ) to bond stretching ( $\alpha$ ) force constant ratio of 0.3 which is representative of chalcogenide materials and well reproduced the observed experimental trends in elastic moduli and phonon density of states for  $\text{Ge}_x\text{Se}_{1-x}$  alloys [124]. However, the  $\beta/\alpha$  ratio for SiC is substantially higher (0.54) [125] due to significantly larger bond bending force constants. Therefore, it is possible that the stronger bond bending forces relative to the weak van der Waal type forces allow the critical coordination singularity to be more apparent in the elastic properties of a-SiC:H.

To further investigate the influence of bond stiffness on the presence of a critical coordination number in the elastic properties of materials, we have examined literature studies of pure group IV amorphous materials such as C, Si or Ge. While there have been a few relevant investigations for a-Si:H, a-Si<sub>x</sub>Ge<sub>1-x</sub>:H, and a-CF<sub>x</sub> alloys [77,82,111], a more compelling and complete data set can be formed from the investigations correlating the elastic properties of organic polymers, and a variety of amorphous carbon (a-C:H) and diamond like carbon (DLC) thin films to hydrogen content, mass density, and sp<sup>2</sup>/sp<sup>3</sup> ratios from which  $\langle r \rangle$  can be directly calculated if not directly reported [127–134]. In Fig. 9, we present a summary of Young's moduli (plotted as E<sup>2/3</sup> vs.  $\langle r \rangle$ ) for a variety of amorphous and amorphous hydrogenated carbon films reported in the literature. As can be seen, the data strongly indicates the presence of a critical point in the vicinity of  $\langle r \rangle \cong 2.2$  similar to our observations for a-SiC:H. Linear regression analysis of the combined data points in Fig. 9, indicates an x-intercept of 2.2 with R<sup>2</sup> = 0.82. Boolchand has shown similar trends in reported hardness data for a-C:H films [110]. Since the C–C bonds in diamond are known to have extremely high stiffness and a  $\beta/\alpha$  ratio of 0.655 [126], the observed singularity at  $\langle r \rangle \cong 2.2$  is consistent with our assertion that experimental observation of a critical coordination may be possible for materials with higher elastic force constants relative to weak van der Waal types forces.

For completeness, we do note that Feng [135] and Nakamura [136] have indirectly observed a stiffness threshold at  $\langle r \rangle = 2.4$ –2.46 in Ge<sub>x</sub>Se<sub>1-x</sub> glasses by monitoring changes in the frequency of optical modes in Raman scattering measurements. Most recently, Wang et al. have also reported to observe two transitions at  $\langle r \rangle = 2.45$  and 2.65 in the shear and compressive elastic moduli of Ge–As–Se glasses using ultrasonic pulse interferometry [137]. Unfortunately for the latter, no explanation was provided by the authors for why the transition at 2.45 was observed and not in the numerous previous studies.

Constraint theory and bond percolation concepts have been previously applied to the interpretation of mechanical properties for other low-*k* materials prepared by similar PECVD routes including a-SiOC:H [56–59], a-SiCN:H [138,139] and a-CF<sub>x</sub> [82,83] low-*k* dielectrics. For these low-*k* dielectrics,  $\langle r \rangle$  was likewise manipulated by intentionally varying the concentration of terminal hydrogen, fluorine and organic groups during either the film deposition [56,82,138] or by post deposition annealing treatments [56,58]. In many of these studies [56–58,82,138,139], the authors have observed a singularity in the vicinity of  $\langle r \rangle = 2.3$ –2.46 for Young's modulus or hardness. These results are consistent with the results of this study and those reported in the literature for a-C:H/DLC films. However as Si–O and Si–N bonds in SiO<sub>2</sub> and Si<sub>3</sub>N<sub>4</sub> have significantly smaller  $\beta/\alpha$  ratios (0.1–0.18) [140–143], this either indicates the magnitude of van der Waal type forces is

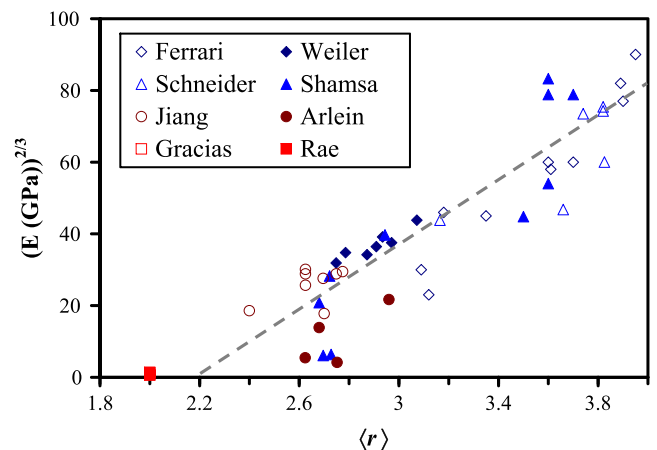


Fig. 9. (Young's modulus)<sup>2/3</sup> vs.  $\langle r \rangle$  for a-C:H, ta-C:H, ta-C, and DLC films reported in the literature.

reduced in these dielectrics or the presence of network (or terminal) Si–C bonding in these materials plays a significant role in allowing the singularity at  $\langle r \rangle_c$  to be observed. It also suggests that bond homogeneity may also be important. For the present study and the results for a-C:H, a-CF<sub>x</sub>, a-SiOC:H, and a-SiCN:H, the primary network bonding remains the same due to  $\langle r \rangle$  being reduced by insertion of terminal H, F or CH<sub>x</sub> groups. For the chalcogenides,  $\langle r \rangle$  is modified by varying the proportion of two, three, and four fold coordinated atoms. This also causes the composition and the related force constants of the network bonds to change with  $\langle r \rangle$ . Such bond heterogeneity could be an additional reason for  $\langle r \rangle_c$  not being observed in the elastic constants and hardness of chalcogenide materials.

Switching to another mechanical related material property, we show included in Fig. 7 the a-SiC:H intrinsic film stress as a function of  $\langle r \rangle$ . As illustrated, the a-SiC:H films exhibit a large compressive stress that decreases with decreasing  $\langle r \rangle$ . At  $\langle r \rangle \cong 2.6$ –2.7, a near neutral stress is achieved and the a-SiC:H film stress becomes weakly tensile and invariant at lower values of  $\langle r \rangle$ . This is somewhat consistent with the ability of the a-SiC:H network to support larger stresses as rigidity percolates through the system with increasing  $\langle r \rangle$ . The inflection point at  $\langle r \rangle \cong 2.6$ –2.7 instead of  $\langle r \rangle = 2.4$  is also suggestive of the presence of an intermediate isostatically rigid or “Booldand” phase [122,123]. However, we caution that the observed stress dependence on  $\langle r \rangle$  may be an artifact of the specific PECVD process conditions utilized to deposit the films with varying hydrogen content. Specifically, low hydrogen content films were primarily achieved by employing increasing amounts of ion bombardment through the application of increased amounts of low frequency (200–400 kHz) RF power [144]. The increased ion bombardment leads to both film densification/decreased hydrogen content and increasingly larger amounts of compressive intrinsic film stress along with increased  $\langle r \rangle$  [42]. Thus, the magnitude of the stress generated in the a-SiC:H films during deposition is both an indication of rigidity percolating through the system and the specific process conditions utilized to deposit and impart stress to the film. This may explain why the difference in the inflection point for Young's modulus versus stress is significantly larger than what has been previously reported for chalcogenide glasses where intermediate phases have been proven to exist. For chalcogenide glasses, the difference in average coordination for the onset of floppy versus rigid isostatic phases ( $\Delta\langle r \rangle$ ) is on the order of 0.1–0.2 [123]. In this study, the difference in the observed  $\Delta\langle r \rangle$  for Young's modulus and intrinsic stress is larger at 0.3–0.4.

The above discussion does explain why a tensile stress is observed for the 3C–SiC on Si epilayer film [88]. In this case, the epilayer film was deposited at higher temperatures by CVD and ion bombardment was accordingly absent. The resulting stress in the epilayer film is therefore primarily a result of the mismatch in lattice constant and thermal expansion coefficient between the Si substrate and the 3C–SiC epilayer [145]. Similarly, the tensile stress for the a-SiC:H films with  $\langle r \rangle < 2.6$  are also likely a result of a mismatch in thermal expansion coefficient with the Si substrate due to a decreased compressive stress component from ion bombardment. We also note that Khakani has previously observed highly compressive PECVD a-SiC:H films to become tensile with simple annealing and some hydrogen loss [146].

A similar dependence of film stress on hydrogen content, ion bombardment, and  $\langle r \rangle$  has also been observed in a-C:H and DLC films deposited by a variety of methods [128]. In these cases, films with even higher compressive stresses (2–5 GPa) have been observed and a direct dependence between ion bombardment, stress, and hydrogen content has been established [147,148]. Similar effects have also been observed in PECVD deposition of SiO<sub>2</sub>, SiN:H, and SiON thin film materials [144].

Due to the large amount of stress shown in Fig. 7 for some of the a-SiC:H films, we also note that Tang and Thorpe [149] have previously shown for a 2D triangular lattice that the critical connectivity is a function of applied tension. Thus it is possible for  $\langle r \rangle_c$  to be both a function of hydrogen content (as shown in Eq. (2)), and the intrinsic film stress.

However for the films closest to the critical point, the tensile stress is quite low (10–40 MPa). Therefore, we expect this effect to be minimal.

### 3.3. Thermal properties

Fig. 10 displays as a function of  $\langle r \rangle$  the values of thermal conductivity ( $\kappa$ ) determined for the a-SiC:H films by TDTR measurements [101]. While thermal conductivity is generally observed to decrease with decreasing  $\langle r \rangle$ , in the present study we find an inflection point at  $\langle r \rangle = 2.4$  and another at  $\langle r \rangle \cong 2.8$ . At lower values of  $\langle r \rangle$  we find very low thermal conductivities and above  $\langle r \rangle = 2.8$  we observe the expected monotonic increase. We observe a general plateau in thermal conductivity from  $\langle r \rangle = 2.4$ –2.8.

Similar inflection points at  $\langle r \rangle = 2.4$  and 2.6–2.7 have been observed for the thermal diffusivity of a variety of binary and ternary chalcogenide glasses [149–154] (it should be noted that thermal diffusivity ( $\alpha$ ) is directly related to thermal conductivity through the relation  $\alpha = \kappa/\rho C_p$  where  $\rho$  is the mass density and  $C_p$  is the heat capacity of the material). For the chalcogenides, the inflection point in thermal diffusivity at  $\langle r \rangle = 2.4$  has been attributed to the same rigidity percolation transition as discussed in the previous section [150,151]. Similarly, the inflection point in thermal diffusivity at  $\langle r \rangle \cong 2.67$  observed in some ternary chalcogenide glasses has been attributed to the medium range chemical ordering effects discussed previously and perhaps the formation of a 2D layered glass structure [152–156].

For the a-SiC:H films investigated in this study, it is tempting to attribute the plateau in thermal conductivity at  $\langle r \rangle = 2.4$ –2.8 to similar medium range ordering effects as observed in chalcogenide glasses. Though if present, such an ordering mechanism must be different. As mentioned previously, the ordering for chalcogenides is a result of achieving a composition that matches that of a discrete thermodynamic chemical compound. For a-SiC:H there are no known stoichiometric compounds in the Si–C–H system beyond SiC. However, referring to Fig. 2, we do note that Si–H bonding in the a-SiC:H films roughly demonstrates a plateau in the region of  $\langle r \rangle = 2.4$ –2.8 with sharp dips on either side. The common plateaus in both Si–H bond density and thermal conductivity in this region could be serendipitous, but could also be related to some other type of medium range ordering. As noted previously, the concentration of terminal Si–CH<sub>3</sub> groups also starts to become increasingly significant below  $\langle r \rangle = 2.6$ . While completely speculative, the thermal conductivity behavior from  $\langle r \rangle = 2.4$ –2.8 could be indicative of a transition from C–SiH<sub>2</sub>–C and Si–CH<sub>2</sub>–Si bonding modes that exhibit some slight increased efficiency for propagating phonon modes to terminal Si–CH<sub>3</sub> species that are clearly inefficient for phonon propagation.

The inflection point in thermal conductivity at  $\langle r \rangle = 2.4$  is also in agreement with prior observations for chalcogenide and a-CF<sub>x</sub> materials

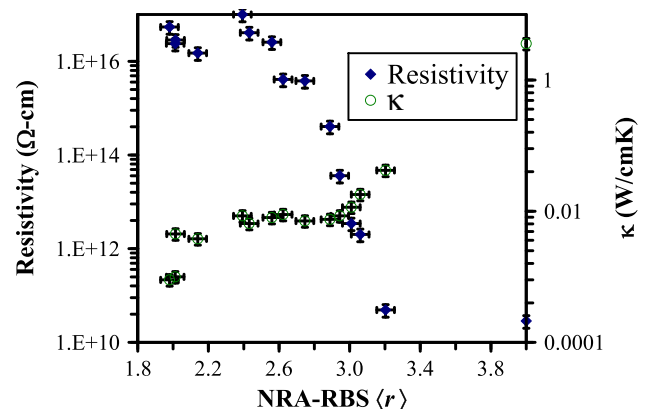


Fig. 10. a-SiC:H thermal conductivity and electrical resistivity vs. NRA-RBS  $\langle r \rangle$ .

[82,150,151]. However, the sharp drop in thermal conductivity at  $\langle r \rangle \cong 2.0$  has not been previously reported to the authors' knowledge. In this case, we believe the reduced thermal conductivity for the films at  $\langle r \rangle \leq 2.0$  is due to the formation of significant amounts of interconnected porosity within the a-SiC:H films [109]. As we will show later, the size and amount of free volume (or pores) in a-SiC:H grow as  $\langle r \rangle$  decreases. At  $\langle r \rangle = 2.0$ , the concentration and diameter of the free volume/pores reach a critical point where interconnected porosity can form across the film and the thermal conductivity of the film can be accurately described using a two phase effective medium approximation [157]. More specifically, the reduced thermal conductivity for films at  $\langle r \rangle \leq 2.0$  is the direct result of a second percolation process in the films, the percolation of pore/free volume interconnectivity instead of a bond percolation process. Based on these results, the critical threshold for porosity appears to be in the vicinity of approximately 5–10%.

For comparison, Fig. 11 shows as a function of  $\langle r \rangle$  a summary of reported thermal conductivity values for another series of organic polymer, a-C:H, ta-C:H, ta-C, and DLC films where  $\langle r \rangle$  was again computed based on the provided hydrogen contents and  $sp^3/sp^2$  ratios [130,132,158–164]. In this case, we observe a sharp drop in thermal conductivity from single crystalline diamond ( $\langle r \rangle = 4.0$ ) to DLC ( $\langle r \rangle = 3.6$ – $3.8$ ) similar to what we observe in Fig. 10 for the transition from 3C–SiC ( $\langle r \rangle = 4.0$ ) to a-SiC:H ( $\langle r \rangle = 3.2$ ). However for DLC/a-C:H, we see a gradual decrease in thermal conductivity from  $\langle r \rangle = 3.6$  down to 2.4 with no clear indications of a plateau near  $\langle r \rangle = 2.4$ – $2.8$ . If such inflection points were to exist for a-C:H as observed in the present study for a-SiC:H, it is certainly possible that it is simply lost in the significant scatter of the reported data. However, saturation in thermal conductivity below  $\langle r \rangle = 2.4$  is observed in the reported a-C:H-DLC data that is consistent with expectations based on constraint theory.

The influence of bond percolation on thermal conductivity has been more clearly demonstrated by Ghossein for a- $CF_x$  thin films [82]. In this case, they observed a clear monotonic decrease in thermal conductivity as  $\langle r \rangle$  decreased from 3.3 to 2.7. Linear extrapolation of the thermal conductivity data to the x-axis indicated a critical coordination number of 2.46 in agreement with the classic constraint theory.

### 3.4. Electrical and optical properties

In Fig. 10, the electrical resistivity of the a-SiC:H films measured at 1 MV/cm is also displayed as a function of  $\langle r \rangle$ . In this case, the resistivity of the films increases with decreasing coordination number and appears to saturate at approximately  $\langle r \rangle = 2.4$ – $2.5$ . This is slightly higher than the critical points observed previously for Young's modulus, hardness, and thermal conductivity where an inflection point was observed to

occur closer to  $\langle r \rangle \cong 2.3$ – $2.4$ . In this case, the saturation in resistance at higher values of  $\langle r \rangle$  could be an artifact of the resistance of the films at  $\langle r \rangle = 2.5$ – $2.6$  exceeding the impedance of the Hg probe utilized for these measurements. However, measurements at higher fields where the films were more conductive showed the same stabilization in resistivity at  $\langle r \rangle = 2.4$ – $2.5$ .

Conductivity percolation has been previously examined both theoretically and experimentally in a number of cases [165–172]. Many theoretical investigations have modeled conductivity as both a bond and site percolation problem [173] by treating a material as an ordered or random array of resistors and sought to predict the critical resistor connectivity or density below which the system effectively represents an open circuit [166–168]. Such depleted resistor network models are analogous to the bond rigidity percolation analysis previously discussed. As one would perhaps expect, Monte Carlo simulations of depleted resistor networks predict a critical resistor density of 39% for a diamond lattice that essentially equates to a critical point at  $\langle r \rangle = 2.4$  [39,166–168]. This is identical to the critical coordination predicted in the rigidity percolation problem. However, experimental investigations and tests of conductivity/resistivity percolation have focused primarily on dopant impurity conduction in semiconductors and two phase granular metal and nanoparticle conductor/insulator matrix systems. Percolation in such conductor/insulator systems is more of a site percolation problem and Monte Carlo simulations in this case predict a slightly higher critical resistor density of 42.5% for a diamond lattice [36,167] which equates to a slightly lower critical coordination of 2.3.

In the present study, we are working with a single phase dielectric where one might initially expect conduction to be a bond percolation problem. However, a previous analysis of the a-SiC:H IV measurements indicates that electron transport through the films with  $\langle r \rangle \geq 2.4$  is via a Frenkel–Poole (FP) mechanism where electrons conduct through the film via point defects or traps in the band gap of the dielectric [174]. In this regard, the observed conductivity percolation in a-SiC:H could be viewed instead as a site percolation problem if electrons must conduct site to site through the point defects. In this case, our observation of a critical point at  $\langle r \rangle = 2.4$ – $2.5$  is further away from that predicted by theory. However, we note that FP conduction is also an electric field activated mechanism where the applied field lowers the barrier height that electrons trapped in point defects must overcome in order to transport through the film. So for an electron to move from one point defect/trap to another there is both a proximity and energy requirement. The additional energy requirement and constraint likely contribute to the observed singularity in resistivity/conductivity for the a-SiC:H films occurring at a slightly higher  $\langle r \rangle$ .

We do note that some general trends in the conductivity/resistivity of a-C:H/DLC [128,175] films and chalcogenide glasses [176,177] have been reported that could also be attributed to average coordination and network connectivity. However in such studies, either insufficient composition data exists to deduce the average coordination  $\langle r \rangle$  [128,175] or an insufficient range in  $\langle r \rangle$  was explored to allow a clear identification of any singularities at  $\langle r \rangle_c$  [176,177].

Fig. 12 displays both the low frequency dielectric constant (100 kHz) and the high frequency optical dielectric constant ( $= RI^2$ ) as a function of  $\langle r \rangle$ . Both the high and low frequency dielectric constants are observed to decrease with decreasing coordination number with the low frequency dielectric constant ranging from a relatively high- $k$  value of 9.7 for single crystalline 3C–SiC down to comparatively low- $k$  values of 2.8–3.2. The low frequency dielectric constant values are also higher than the high frequency dielectric constant by approximately a value of one for most films. This is due to the fact that the low frequency dielectric constant is a function of both electronic, ionic, and bond dipole configuration terms whereas the high frequency dielectric constant is a function of only electronic contributions [178]. If the bonding in Si–C was purely covalent, the high and low frequency dielectric constants would be expected to be the same. However, Si–C bonding is partially ionic [179], so there is a contribution to the low frequency dielectric constant

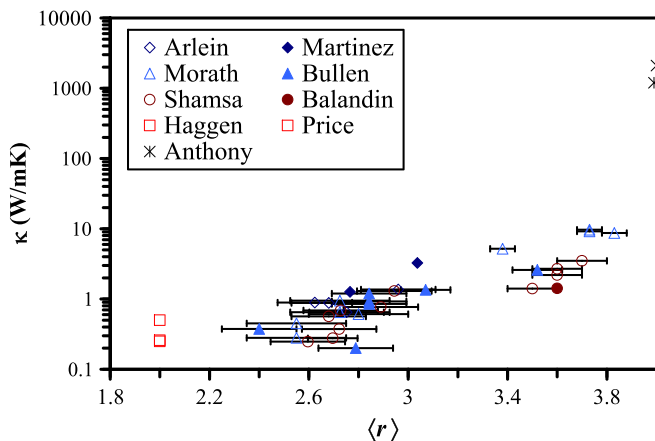


Fig. 11. Thermal conductivity vs.  $\langle r \rangle$  for a-C:H, ta-C:H, ta-C, and DLC films reported in the literature.

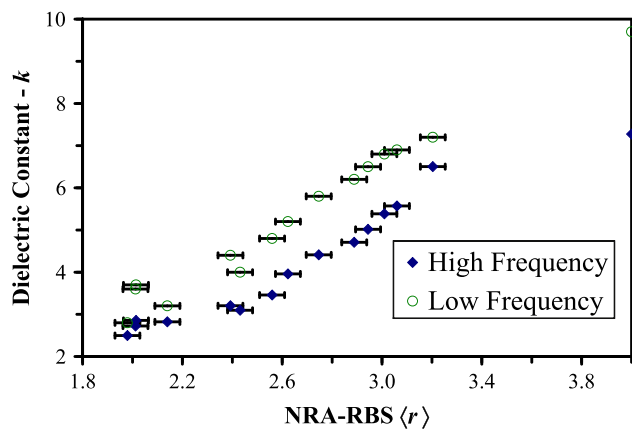


Fig. 12. a-SiC:H high frequency and low frequency dielectric constant vs. NRA-RBS ( $r$ ).

that drops out at optical frequencies. For the two films where the low and high frequency dielectric constants are within 0.35 of one another, we note that these films are ~80% carbon and could therefore be considered to have increased covalent C–C bonding. The increased covalent bonding decreases the ionic contribution and brings the low and high frequency dielectric constants into close agreement with one another.

In Fig. 12, a possible inflection point in the vicinity of  $\langle r \rangle \cong 2.3$  can be noted for both the low and high frequency dielectric constants. While there have been several reports of critical points in the dielectric properties of two phase systems, to the author's knowledge, there have been no such reports for single phase systems either theoretically or experimentally. In fact, effective medium theory would predict a smooth variation in optical properties across the Si–C–H phase diagram [76]. Likewise, studies of the dielectric properties in chalcogenide glasses have only shown singularities or inflections at values of  $\langle r \rangle$  that correspond to the composition of stoichiometric equilibrium phases [180]. In this case, it is important to note that for two of the films at  $\langle r \rangle < 2.4$ , there is a sudden change in stoichiometry from a C/Si ratio of ~1 to a C/Si ratio of  $>3$ . Even excluding those two films, there is still a discontinuity in dielectric constant vs.  $\langle r \rangle$  at  $\langle r \rangle < 2.4$ . As we will show next, the observed inflection point in dielectric properties is likely the result of the appearance of a second phase (i.e. interconnected porosity) in the a-SiC:H film at  $\langle r \rangle < 2.4$ .

### 3.5. Other physical properties

Fig. 13 displays the XRR mass density and the EP% porosity as a function of  $\langle r \rangle$ . As with other properties, an inflection point at  $\langle r \rangle \cong 2.3$  is observed in both sets of data. The mass density was observed to become less dependent on  $\langle r \rangle$  for values  $< 2.4$ , whereas for  $\langle r \rangle \geq 2.4$  no interconnected porosity was detected by EP using toluene as a diffusing solvent. This is consistent with the trends observed in the dielectric constant data previously where  $k$  was observed to become comparatively invariant at  $\langle r \rangle < \cong 2.3$  and confirms the previous assertion that the inflection point in  $k$  corresponds with the beginning of interconnected porosity percolation in the a-SiC:H films. It also coincides with the steep drop in thermal conductivity observed for the two a-SiC:H films with  $\langle r \rangle = 2.0$ .

However, PALS measurements by Zambov [181] have shown that some level of nano-porosity likely exists in all of the a-SiC:H films investigated in the present study. For our samples, no positronium formation was observed for the single crystal 3C–SiC sample and the highest density/ $\langle r \rangle$  a-SiC:H sample, but positronium formation was detected with steadily increasing lifetimes as  $\langle r \rangle$  decreased below 3.2. The average pore sizes deduced from continuum fitting of the positronium lifetime spectra are shown in Fig. 14. As can be seen, the deduced average pore size increases from 0.3 nm to 0.85 nm with decreasing coordination until  $\langle r \rangle \cong 2.4$  is reached. Below  $\langle r \rangle = 2.4$  there is relatively little change

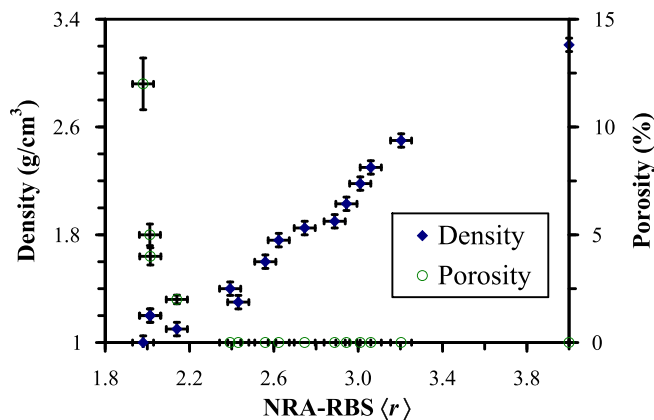


Fig. 13. a-SiC:H XRR mass density and EP % porosity vs. NRA-RBS ( $r$ ).

in the median pore diameter. The development and increase in interconnected porosity detected by toluene EP are therefore likely a result of either an increase in the total volume of pores or an increase in the pore size distribution. The data in Figs. 13 and 14 confirm that the trends observed in Fig. 12 for the a-SiC:H dielectric properties are indeed due to the creation and eventual percolation of free volume/porosity.

## 4. Constraint theory and bond percolation implications for future low- $k$ materials

As mentioned previously, prior applications of constraint theory concepts to low- $k$  dielectrics have focused solely on the impact of bond percolation on mechanical properties such as Young's modulus, hardness, and fracture energy/toughness [56–59]. As we have shown above, network bond percolation has an underlying role in all material properties including mechanical, thermal, electrical, and optical. In almost all cases, decreasing  $\langle r \rangle$  to reduce the dielectric constant results in a rapid deterioration of the other material properties that is quite sobering from a device standpoint. The only case observed here where decreasing  $\langle r \rangle$  works to one's advantage from an insulating dielectric perspective is the observed increase in resistivity with decreased network connectivity. Therefore, the above results clearly illustrate the well known tradeoff in low- $k$  dielectrics where gains in reducing dielectric constant are tempered by a reduction in other important material properties [1,2]. However, they also highlight network connectivity as an important fundamental underlying consideration. Although not always clearly demonstrated or articulated, most of the claimed improvements in low- $k$  mechanical properties achieved via new

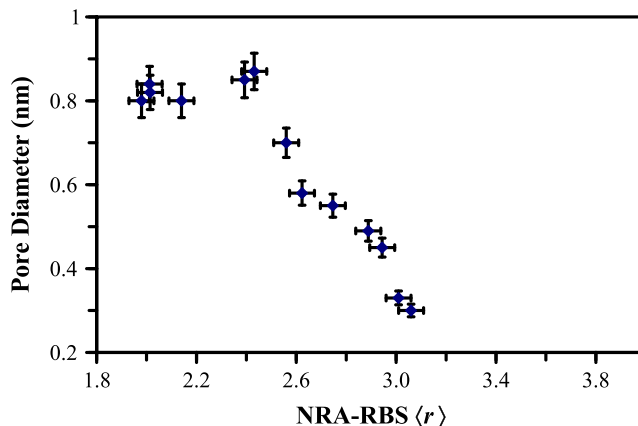


Fig. 14. a-SiC:H PALS pore diameter vs.  $\langle r \rangle$ .

precursors [182,183], post deposition annealing [57], and electron/UV curing [86] are likely a result of increased network connectivity.

While constraint theory/bond percolation may seem to make the challenge of achieving new low- $k$  materials with improved properties quite daunting, it does also provide some added insight for possible future directions. Typically, the primary research goal for new low- $k$  materials is to achieve the lowest possible  $k$  with the highest possible mechanical properties. Bond percolation theory clearly indicates that the current methods for reducing  $k$  via incorporation of terminal hydrogen or organic groups will directly result in a corresponding reduction in elastic constants and hardness of the material while one is above  $\langle r \rangle_c$ . However, this can be tempered somewhat by intentionally incorporating network bonds with increased stiffness and/or bonds with similar stiffness but lower polarizability. In this regard, it is perhaps not too surprising that there have been several reports in the literature of attempts to improve the mechanical properties of low- $k$  SiOC:H dielectrics by intentionally replacing Si–O–Si bonds with stiffer Si–C–Si bonds [184,185].

As one goes below  $\langle r \rangle_c$ , low- $k$  mechanical properties, however, should become invariant with further reductions in  $\langle r \rangle$ . Thus below  $\langle r \rangle_c$ , it may be possible to achieve continued reductions in  $k$  while not suffering continued reductions in mechanical properties. In this regard, it is important to note that below  $\langle r \rangle_c$  the elastic properties of a material are more dominated by weak van der Waal type forces. Thus in addition to focusing on achieving improvements in mechanical properties via the incorporation of stiffer network bonds (as in the replacement of Si–O–Si with Si–C–Si bonds in low- $k$  SiOC:H dielectrics noted above), it may also be important to focus on means for increasing the magnitude of weaker van der Waal types forces in low- $k$  materials. Along these lines, we note that the recent molecular dynamic simulations by Li et al. [59] have shown that the presence of terminal CH<sub>3</sub> versus OH groups can have a marked effect on the bulk and shear modulus of low- $k$  SiOC:H dielectrics with  $\langle r \rangle$  in the range of 2.2–2.7.

It is also important to note that below  $\langle r \rangle_c$  a material is under constrained and from the perspective of constraint theory considered “flexible” or “deformable” [23,25]. While mechanical properties such as Young’s modulus and hardness may be at a minimum, other important mechanical properties such as fracture toughness may actually increase and improve should the remaining network bonding have enough flexibility to accommodate significant deformation. Thus, another possible path for improving low- $k$  dielectric mechanical properties could be the strategic inclusion of deformable C–C–C network chains [84,98]. The unintentional [186] and intentional [187] incorporation of such C–C–C linkages has already been shown to dramatically improve the fracture properties of low- $k$  SiOC:H dielectrics.

While constraint theory predicts that material properties should remain invariant with  $\langle r \rangle$  below  $\langle r \rangle_c$ , Fig. 13 illustrates that there are additional considerations. Specifically, significant interconnected porosity can start to form in the material and cause further significant reductions in the dielectric material properties. The data in Fig. 13 suggests that  $\langle r \rangle_c$  is also the critical point for a second type of percolation phenomena – the percolation of interconnected nano-pores. However, the percolation of interconnected porosity can also again result in significant deterioration of material properties. As shown in Fig. 10, a significant reduction in thermal conductivity occurred once interconnected porosity was formed. While not apparent in the Young’s modulus and hardness results presented here, percolation of interconnected porosity can also lead to reductions in these properties once pores of significant size and interconnectivity are formed. Factoring in both combined bond and pore percolation, perhaps the optimum or most desirable network connectivity for a material from a low- $k$  perspective is the minimum coordination at which interconnected porosity forms.

Lastly, it is interesting to look at the opposite of low- $k$  materials, i.e. high- $k$  materials from a constraint theory and bond percolation perspective. In this case, everything generally lines up in ones favor in terms of mechanical, thermal, and optical properties except for

resistivity. In this case, we note that bond percolation theory and the results presented in Fig. 10 illustrate that some significant gains in resistivity/electrical leakage could perhaps be achieved if one is willing to accept a reduction in dielectric constant to slightly reduce network connectivity and perhaps passivate some point defects that are known to limit high- $k$  dielectric reliability [188].

## 5. Conclusions

Combined NRA, RBS, NMR and FTIR measurements have been utilized to determine the average coordination ( $\langle r \rangle$ ) and network connectivity ( $\langle r \rangle_{\text{net}}$ ) for a series of PECVD a-SiC:H films. The changes in  $\langle r \rangle$  have been correlated to the full mechanical, thermal, electrical, optical, and physical properties for a-SiC:H. The results clearly show that the observed variation in a-SiC:H properties can be fully explained by constraint theory and bond percolation concepts. Most importantly, singularities are observed in all the material properties close to the critical coordination predicted by constraint theory. These results highlight the fact that bond percolation/network connectivity is an important factor and underlying consideration for the optimization of all properties in future low- $k$  and high- $k$  materials.

## Acknowledgements

The authors would like to acknowledge additional NMR measurements by Drs Asher Schmidt and Shifi Kababya of the Schulich Faculty of Chemistry at Technion, Israel Institute of Technology. The authors would also like to acknowledge Drs. Jeff Armstrong, Marc French, Ebony Mays, Prahalad Parthangal, Boyan Boyanov, Jose Maiz, Robert McFadden, James Roesler, and Bruce Tufts of Intel for their thoughtful discussion, support for this research and help in preparing the manuscript.

## References

- [1] K. Maex, M.R. Baklanov, D. Shamiryan, F. Iacopi, S.H. Brongersma, Z.S. Yanovitskaya, *J. Appl. Phys.* 93 (2003) 8793.
- [2] W. Volksen, R. Miller, G. Dubois, *Chem. Rev.* 110 (2010) 56.
- [3] H. Treichel, *J. Electron. Mater.* 30 (2001) 290.
- [4] A. Lee, N. Rajagopalan, M. Le, B. Kim, H. M'Saad, *J. Electrochem. Soc.* 151 (2004) F7.
- [5] D. Gan, P. Ho, Y. Pang, R. Huang, J. Leu, J. Maiz, T. Scherban, *J. Mater. Res.* 21 (2006) 1512.
- [6] T. Wang, Y. Cheng, Y. Wang, T. Hsieh, G. Hwang, C. Chen, *Thin Solid Films* 498 (2006) 36.
- [7] K. Kuhn, *Microelectron. Eng.* 88 (2011) 1044.
- [8] E. Andideh, M. Lerner, G. Palmrose, S. El-Mansy, T. Scherban, G. Xu, J. Blaine, *J. Vac. Sci. Technol. B* 22 (2004) 196.
- [9] A. Volinsky, J. Vella, W. Gerberich, *Thin Solid Films* 429 (2003) 201.
- [10] A. Padovani, L. Rhodes, L. Riestler, G. Lohman, B. Tsuie, J. Conner, S. Allen, P. Kohl, *Electrochem. Solid-State Lett.* 4 (2001) F25.
- [11] E. Besien, M. Pantouvaki, L. Zhao, D. De Roest, M. Baklanov, Z. Tokei, G. Beyer, *Microelectron. Eng.* 92 (2012) 59.
- [12] G. Haase, *J. Appl. Phys.* 105 (2009) 44908.
- [13] B. Daly, H. Maris, W. Ford, G. Antonelli, L. Wong, E. Andideh, *J. Appl. Phys.* 92 (2002) 6005.
- [14] A. Delan, M. Rennau, S. Schulz, T. Gessner, *Microelectron. Eng.* 70 (2003) 280.
- [15] T. Furusawa, D. Ryuzaki, R. Yoneyama, Y. Homma, K. Hinode, *J. Electrochem. Soc.* 148 (2001) F175.
- [16] F. Iacopi, S. Brongersma, B. Vandeveld, M. O'Toole, D. Degryse, Y. Travaly, K. Maex, *Microelectron. Eng.* 75 (2004) 54.
- [17] M. Hussein, J. He, *IEEE Trans. Semicond. Manuf.* 18 (2005) 69.
- [18] International Technology Roadmap for Semiconductors (ITRS), Semiconductor Industry Association, San Jose, CA, 2011. (see also <http://www.itrs.net/Links/2011ITRS/Home2011.htm>).
- [19] H. Yoo, S. Balakrishnan, J. Bielefeld, M. Harmes, H. Hiramatsu, S. King, M. Kobrinsky, B. Krist, P. Reese, V. RamachandraRao, K. Singh, C. Suri, C. Ward, *Proc. IEEE Int. Interconnect. Conf.*, 2010.
- [20] T. Frot, W. Volksen, S. Purushothaman, R. Bruce, T. Magbitang, D. Miller, D. Vaughn, G. Dubois, *Adv. Funct. Mater.* 22 (2012) 1.
- [21] J. Mauro, *Am. Ceram. Soc. Bull.* 90 (2011) 31.
- [22] J. Phillips, *J. Non-Cryst. Solids* 34 (1979) 153.
- [23] J. Phillips, M. Thorpe, *Solid State Commun.* 53 (1985) 699.
- [24] G. Dohler, R. Dandolo, H. Bilz, *J. Non-Cryst. Solids* 42 (1980) 87.
- [25] M. Thorpe, *J. Non-Cryst. Solids* 57 (1983) 355.
- [26] P. Gupta, A. Cooper, *J. Non-Cryst. Solids* 123 (1990) 14.
- [27] H. He, M. Thorpe, *Phys. Rev. Lett.* 54 (1985) 2107.

- [28] E. Garboczi, M. Thorpe, *Phys. Rev. B* 31 (1985) 7276.
- [29] S. Feng, B. Halperin, P. Sen, *Phys. Rev. B* 35 (1987) 197.
- [30] D. Franzblau, J. Tersoff, *Phys. Rev. Lett.* 68 (1992) 2172.
- [31] W. Tang, M. Thorpe, *Phys. Rev. B* 42 (1990) 3798.
- [32] M. Sahimi, J. Goddard, *Phys. Rev. B* 33 (1986) 7848.
- [33] M. Sahimi, S. Arbabi, *MRS Proc.* 207 (1991) 201.
- [34] S. Zhang, C. Lung, K. Wang, *Phys. Rev. B* 42 (1990) 6631.
- [35] P. Duxbury, P. Leath, P. Beale, *Phys. Rev. B* 36 (1987) 367.
- [36] H. Frisch, E. Sonnenblick, V. Vyssotsky, J. Hammersley, *Phys. Rev.* 124 (1961) 1021.
- [37] V. Vyssotsky, S. Gordon, H. Frisch, J. Hammersley, *Phys. Rev.* 123 (1961) 1566.
- [38] M. Thorpe, *J. Non-Cryst. Solids* 182 (1995) 135.
- [39] M. Thorpe, D. Jacobs, M. Chubynsky, J. Phillips, *J. Non-Cryst. Solids* 266 (2000) 859.
- [40] J. Phillips, *Phys. Rev. B* 31 (1985) 8157.
- [41] N. Tajima, T. Ohno, T. Hamada, K. Yoneda, S. Kondo, N. Kobayashi, M. Shiriki, Y. Inaishi, K. Miyazawa, K. Sakota, S. Hasaka, M. Inoue, *Jpn. J. Appl. Phys.* 46 (2007) 5970.
- [42] S. King, M. French, J. Bielefeld, W. Lanford, *J. Non-Cryst. Solids* 357 (2011) 2970.
- [43] S. King, G. Antonelli, *Thin Solid Films* 515 (2007) 7232.
- [44] S. King, J. Bielefeld, *ECS Trans.* 33 (2010) 185.
- [45] J. Mauro, P. Gupta, R. Loucks, *J. Chem. Phys.* 130 (2009) 234503.
- [46] M. Smedskjaer, J. Mauro, S. Sen, Y. Yue, *Chem. Mater.* 22 (2010) 5358.
- [47] M. Smedskjaer, J. Mauro, Y. Yue, *Phys. Rev. Lett.* 105 (2010) 115503.
- [48] K. Tanaka, *Solid State Commun.* 54 (1985) 867.
- [49] U. Senapati, A. Varshneya, *J. Non-Cryst. Solids* 185 (1995) 289.
- [50] A. Varshneya, *J. Non-Cryst. Solids* 273 (2000) 1.
- [51] P. Gupta, J. Mauro, *J. Chem. Phys.* 130 (2009) 94503.
- [52] P. Boolchand, M. Thorpe, *Phys. Rev. B* 50 (1994) 10366.
- [53] X. Feng, W. Bresser, M. Zhang, B. Goodman, P. Boolchand, *J. Non-Cryst. Solids* 222 (1997) 137.
- [54] J. Mauro, A. Varshneya, *J. Am. Ceram. Soc.* 90 (2007) 192.
- [55] P. Gupta, D. Miracle, *Acta Mater.* 55 (2007) 4507.
- [56] D. Burkley, K. Gleason, *J. Appl. Phys.* 93 (2003) 5143.
- [57] A. Ross, K. Gleason, *J. Appl. Phys.* 97 (2005) 113707.
- [58] N. Trujillo, Q. Wu, K. Gleason, *Adv. Funct. Mater.* 20 (2010) 607.
- [59] H. Li, J. Knap, E. Kaxiras, J. Vlassak, *Acta Mater.* 59 (2011) 44.
- [60] P. Wang, Z. Wu, T. Lu, L. Interrante, *J. Electrochem. Soc.* 153 (2006) G267.
- [61] Y. Matsuda, J. Rathmore, L. Interrante, R. Dauskardt, G. Dubois, *Appl. Mater. Interfaces* 4 (2012) 2659.
- [62] M. Baklanov, M. Van Hove, G. Mannaert, S. Vanhaelemeersch, H. Bender, T. Conard, K. Maex, *J. Vac. Sci. Technol. B* 18 (2000) 1281.
- [63] C. Alfred, V. Jousseume, *Surf. Coat. Technol.* 201 (2007) 9260.
- [64] M. Loboda, *Microelectron. Eng.* 50 (2000) 15.
- [65] C. Chiang, M. Chen, C. Ko, Z. Wu, S. Jang, M. Liang, *Jpn. J. Appl. Phys.* 42 (2003) 4273.
- [66] C. Chiang, M. Chen, C. Ko, S. Jang, C. Yu, M. Liang, *Jpn. J. Appl. Phys.* 42 (2004) 5246.
- [67] Y. Cheng, J. Wu, T. Chiu, S. Chen, Y. Wang, *J. Vac. Sci. Technol. B* 29 (2011) 31207.
- [68] A. Mallikarjunan, A. Johnson, L. Matz, R. Vrtis, A. Kovacs, X. Jiang, M. Xiao, *Microelectron. Eng.* 92 (2012) 83.
- [69] N. Ledermann, J. Baborowski, P. Murali, N. Xantopoulos, J. Tellenbach, *Surf. Coat. Technol.* 125 (2000) 246.
- [70] A. Jean, M. Chaker, Y. Diawara, P. Leung, E. Gat, P. Mercier, H. Pepin, S. Gujrathi, G. Ross, J. Kieffer, *J. Appl. Phys.* 72 (1992) 3110.
- [71] S. Cogan, D. Edell, A. Guzelian, Y. Liu, R. Edell, *J. Biomed. Mater. Res. A* 67A (2003) 856.
- [72] D. Wu, R. Horng, C. Chan, Y. Lee, *Appl. Surf. Sci.* 144 (1999) 708.
- [73] M. Loboda, J. Seifferly, F. Dall, *J. Vac. Sci. Technol. A* 12 (1994) 90.
- [74] S. Myong, S. Kim, K. Lim, *J. Appl. Phys.* 95 (2004) 1525.
- [75] T. Chang, Y. Chu, C. Lee, J. Chang, *Appl. Phys. Lett.* 101 (2012) 241601.
- [76] K. Mui, D. Basa, F. Smith, R. Corderman, *Phys. Rev. B* 35 (1987) 8089.
- [77] R. Kuschnerit, H. Fath, A. Kolomenskii, M. Szabadi, P. Hess, *Appl. Phys. A* 61 (1995) 269.
- [78] X. Jiang, K. Reichelt, B. Stritzker, *J. Appl. Phys.* 66 (1989) 5805.
- [79] B. Dischler, A. Bubenzer, P. Koidl, *Solid State Commun.* 48 (1983) 105.
- [80] J. Robertson, *Phys. Rev. Lett.* 68 (1992) 220.
- [81] J. Angus, F. Jansen, *J. Vac. Sci. Technol. A* 6 (1988) 1778.
- [82] M. Ghossoub, J. Lee, O. Baris, D. Cahill, S. Sinha, *Phys. Rev. B* 82 (2010) 195441.
- [83] J. Perrin, R. Dandoloff, *J. Non-Cryst. Solids* 86 (1986) 179.
- [84] Y. Matsuda, S. King, J. Bielefeld, J. Xu, R. Dauskardt, *Acta Mater.* 60 (2012) 682.
- [85] Y. Matsuda, S. King, M. Oliver, R. Dauskardt, *J. Appl. Phys.* 113 (2013) 83521.
- [86] V. Jousseume, A. Zenasni, L. Favanne, G. Gerbaud, M. Bardet, J. Simon, A. Humbert, *J. Electrochem. Soc.* 154 (2007) G103.
- [87] W. Gray, M. Loboda, J. Bremmer, H. Struyf, M. Lepage, M. Van Hove, R. Donaton, E. Slecckx, M. Stucchi, F. Lanckmans, T. Gao, W. Boullart, B. Coenegrachts, M. Maenhoudt, S. Vanhaelemeersch, H. Meynen, K. Maex, *J. Electrochem. Soc.* 150 (2003) G404.
- [88] C. Locke, R. Anzalone, A. Severino, C. Bongiorno, G. Litrico, F. La Via, S.E. Sadow, *Material, Science Forum*, 615–617, 2009, p. 145.
- [89] Certain commercial equipment, instruments or materials are identified in this document. Such identification does not imply recommendation or endorsement by Intel Corporation or the National Institute of Standards and Technology, nor does it imply that the products identified are necessary the best available for the purpose.
- [90] W.A. Lanford, in: J. Tesmer, M. Nastasi (Eds.), *Handbook of Modern Ion Beam Analysis*, MRS, Pittsburgh, 1995, (Chapter 8).
- [91] G. Vizkelethy, in: J. Tesmer, M. Nastasi (Eds.), *Handbook of Modern Ion Beam Analysis*, MRS, Pittsburgh, 1995, (Chapter 6).
- [92] W.A. Lanford, in: Y. Wang, M. Nastasi (Eds.), *Handbook of Modern Ion Beam Analysis*, 2nd edition, MRS, Pittsburgh, 2009, p. 175.
- [93] L.R. Doolittle, *Nucl. Instrum. Methods Phys. Res. B* 89 (1985) 344.
- [94] S. King, J. Bielefeld, M. French, W. Lanford, *J. Non-Cryst. Solids* 357 (2011) 3602.
- [95] S. King, J. Bielefeld, M. French, W. Lanford, *J. Non-Cryst. Solids* (2013), <http://dx.doi.org/10.1016/j.jnoncrysol.2013.06.021> (accepted for publication).
- [96] D. Gage, J. Stebbins, L. Peng, Z. Cui, A. Al-Bayati, K. MacWilliams, H. M'Saad, R. Dauskardt, *J. Appl. Phys.* 104 (2008) 43513.
- [97] Q. Wu, K. Gleason, *J. Vac. Sci. Technol. A* 21 (2003) 388.
- [98] Y. Matsuda, N. Kim, S. King, J. Bielefeld, J. Stebbins, R. Dauskardt, *ACS Appl. Mater. Interfaces* (2013), <http://dx.doi.org/10.1021/am402046e> (submitted for publication).
- [99] S. King, G. Xu, R. Chu, J. Huening, *Thin Solid Films* 518 (2010) 4898.
- [100] G. Stan, S. King, R. Cook, *J. Mater. Res.* 24 (2009) 2960.
- [101] B. Daly, S. Bailey, R. Sooryakumar, S. King, *J. Nanophotonics* 7 (2013) 73094.
- [102] D. Hondongwa, L. Olasov, B. Daly, S. King, J. Bielefeld, *Thin Solid Films* 519 (2011) 7895.
- [103] S. King, J. Gradner, *Micro. Rel.* 49 (2009) 721.
- [104] S. King, *J. Vac. Sci. Technol. A* 29 (2011) 41501.
- [105] S. King, M. French, J. Jaehnic, M. Kuhn, B. Boyanov, B. French, *J. Vac. Sci. Technol. B* 29 (2011) 51207.
- [106] G. Janssen, M. Abdalla, F. van Keulen, B. Pujada, B. van Venrooy, *Thin Solid Films* 517 (2009) 1858.
- [107] M. Baklanov, K. Mogilnikov, V. Polovinkin, N. Dultsev, *J. Vac. Sci. Technol. B* 18 (2000) 1385.
- [108] D. Gidley, H. Peng, R. Vallery, *Annu. Rev. Mater. Res.* 36 (2006) 49.
- [109] S. King, D. Jacob, D. Vanleuven, B. Colvin, J. Kelly, M. French, J. Bielefeld, D. Dutta, M. Liu, D. Gidley, *ECS J. Solid State Sci. Technol.* 1 (2012) N115.
- [110] P. Boolchand, M. Zhang, B. Goodman, *Phys. Rev. B* 53 (1996) 11488.
- [111] N. Mousseau, M. Thorpe, *Phys. Rev. B* 48 (1993) 5172.
- [112] H. Efstathiadis, Z. Yin, F. Smith, *Phys. Rev. B* 46 (1992) 13119.
- [113] B. Halfpap, S. Lindsay, *Phys. Rev. Lett.* 57 (1986) 847.
- [114] S. Yun, H. Li, R. Cappelletti, R. Enzweiler, P. Boolchand, *Phys. Rev. B* 39 (1989) 8702.
- [115] M. Tatsumisago, B. Halfpap, J. Green, S. Lindsay, C. Angell, *Phys. Rev. Lett.* 64 (1990) 1549.
- [116] D. Swiler, A. Varshneya, R. Callahan, *J. Non-Cryst. Solids* 125 (1990) 250.
- [117] W. Kamitakahara, R. Cappelletti, P. Boolchand, B. Halfpap, F. Gompf, D. Neumann, H. Mutka, *Phys. Rev. B* 44 (1991) 94.
- [118] A. Sreeram, A. Varshneya, D. Swiler, *J. Non-Cryst. Solids* 130 (1991) 225.
- [119] K. Tanaka, *Solid State Commun.* 60 (1986) 295.
- [120] K. Tanaka, *Phys. Rev. B* 39 (1989) 1270.
- [121] Y. Wang, P. Boolchand, M. Micoulaut, *Europhys. Lett.* 52 (2000) 633.
- [122] P. Boolchand, X. Feng, W. Bresser, *J. Non-Cryst. Solids* 293 (2001) 348.
- [123] M. Micoulaut, J. Phillips, *J. Non-Cryst. Solids* 353 (2007) 1732.
- [124] U. Senapati, K. Firstenberg, A. Varshneya, *J. Non-Cryst. Solids* 222 (1997) 153.
- [125] Y. Cai, M. Thorpe, *Phys. Rev. B* 40 (1989) 10535.
- [126] J. Martins, A. Zunger, *Phys. Rev. B* 30 (1984) 6217.
- [127] A. Ferrari, J. Robertson, M. Beghi, C. Bottani, R. Ferulano, R. Pastorelli, *Appl. Phys. Lett.* 75 (1999) 1893.
- [128] M. Weiler, S. Sattel, T. Giessen, K. Jung, H. Ehrhardt, V. Veerasamy, J. Robertson, *Phys. Rev. B* 53 (1996) 1594.
- [129] D. Schneider, C. Meyer, H. Mai, B. Schoneich, H. Ziegele, H. Scheibe, Y. Lifshitz, *Diamond Relat. Mater.* 7 (1998) 973.
- [130] M. Shamsa, W. Liu, A. Balandin, C. Casiraghi, W. Milne, A. Ferrari, *Appl. Phys. Lett.* 89 (2006) 161921.
- [131] X. Jiang, *Phys. Rev. B* 43 (1991) 2372.
- [132] J. Arlein, S. Palaich, B. Daly, P. Subramonium, G. Antonelli, *J. Appl. Phys.* 104 (2008) 33508.
- [133] D. Gracias, G. Somorjai, *Macromolecules* 31 (1998) 1269.
- [134] P. Rae, D. Dattelbaum, *Polymer* 45 (2004) 7615.
- [135] X. Feng, W. Bresser, P. Boolchand, *Phys. Rev. Lett.* 78 (1997) 4422.
- [136] M. Nakamura, O. Matsuda, M. Murase, *Phys. Rev. B* 57 (1998) 10228.
- [137] R. Wang, A. Smith, B. Luther-Davies, H. Kokkonen, I. Jackson, *J. Appl. Phys.* 105 (2009) 56109.
- [138] K. Gerstenberg, K. Taube, *Fresenius Z. Anal. Chem.* 333 (1989) 313.
- [139] K. Gerstenberg, *Colloid Polym. Sci.* 268 (1990) 345.
- [140] S. Limb, K. Gleason, D. Edell, E. Gleason, *J. Vac. Sci. Technol. A* 15 (1997) 1814.
- [141] F. Galeener, *Phys. Rev. B* 19 (1979) 4292.
- [142] G. Lucovsky, J. Yang, S. Chao, J. Tyler, W. Czubatyi, *Phys. Rev. B* 28 (1983) 3234.
- [143] J. Wendel, W. Goddard, *J. Chem. Phys.* 97 (1992) 5048.
- [144] W. Claessen, *Plasma Chem. Plasma Polym. J.* 7 (1987) 109.
- [145] D. Talwar, J. Sherbondy, *Appl. Phys. Lett.* 67 (1995) 3301.
- [146] M. Khakani, M. Chaker, A. Jean, S. Boily, H. Pepin, J. Kieffer, S. Gujrathi, *J. Appl. Phys.* 74 (1993) 2834.
- [147] R. Lacerda, F. Marques, *Appl. Phys. Lett.* 73 (1998) 617.
- [148] S. Kumar, P. Dixit, D. Sarangi, R. Bhattacharyya, *J. Appl. Phys.* 85 (1999) 3866.
- [149] W. Tang, M. Thorpe, *Phys. Rev. B* 37 (1988) 5539.
- [150] J. de Lima, N. Cella, L. Miranda, C. Chying An, A. Franzan, N. Leite, *Phys. Rev. B* 46 (1992) 14186.
- [151] J. Philip, K. Madhusoodanan, *Phys. Rev. B* 38 (1988) 4127.
- [152] K. Madhusoodanan, J. Philip, *Phys. Rev. B* 39 (1989) 7922.
- [153] K. Nandakumar, J. Philip, *J. Non-Cryst. Solids* 144 (1992) 247.
- [154] A. Srinivasan, K. Madhusoodanan, E. Gopal, *Solid State Commun.* 83 (1992) 163.
- [155] T. Velinon, M. Gateshki, D. Arsova, E. Vateva, *Phys. Rev. B* 55 (1997) 11014.
- [156] K. Ganesan, K. Madhusoodanan, A. Srinivasan, K. Sangunni, E. Gopal, *Phys. Status Solidi B* 212 (1999) 223.
- [157] J. Liu, D. Gan, C. Hu, M. Kiene, P. Ho, W. Volksen, R. Miller, *Appl. Phys. Lett.* 81 (2002) 4180.
- [158] I. Saurez-Martinez, N. Marks, *Appl. Phys. Lett.* 99 (2011) 33101.

- [159] C. Morath, H. Maris, J. Cuomo, D. Pappas, A. Grill, V. Patel, J. Doyle, J. Appl. Phys. 76 (1994) 2636.
- [160] A. Bullen, K. O'Hara, D. Cahill, O. Monteiro, A. von Keudell, J. Appl. Phys. 88 (2000) 6317.
- [161] A. Balandin, M. Shamsa, W. Liu, C. Casiraghi, A. Ferrari, Appl. Phys. Lett. 93 (2008) 43115.
- [162] R. Haggemueller, C. Guthy, J. Lukes, J. Fischer, K. Winey, Macromolecules 40 (2007) 2417.
- [163] D. Price, M. Jarratt, Thermochim. Acta 392 (2002) 231.
- [164] T. Anthony, W. Banholzer, J. Fleischer, L. Wei, P. Kuo, R. Thomas, R. Pryor, Phys. Rev. B 42 (1990) 1104.
- [165] S. Kirkpatrick, Rev. Mod. Phys. 45 (1973) 574.
- [166] S. Kirkpatrick, Phys. Rev. Lett. 27 (1971) 1722.
- [167] M. Sykes, J. Essam, Phys. Rev. 133 (1964) A310.
- [168] J. Bernasconi, Phys. Rev. B 18 (1978) 2185.
- [169] B. Abeles, H. Pinch, J. Gittleman, Phys. Rev. Lett. 35 (1975) 247.
- [170] I. Balberg, E. Savir, J. Jedrzejewski, A. Nassiopoulou, S. Gardelis, Phys. Rev. B 75 (2007) 235329.
- [171] S. Barrau, P. Demont, A. Peigney, C. Laurent, C. Lacabanne, Macromolecules 36 (2003) 5187.
- [172] Z. Rubin, S. Sunshine, M. Heaney, I. Bloom, I. Balberg, Phys. Rev. B 59 (1999) 12196.
- [173] R. Zallen, The Physics of Amorphous Solids, Wiley, NY, 1983.
- [174] T. Pomorski, B. Bittel, C. Cochrane, P. Lenahan, J. Bielefeld, S. King, J. Appl. Phys. (2013), <http://dx.doi.org/10.1063/1.4818480> (accepted for publication).
- [175] P. Fallon, V. Veerasamy, C. Davis, J. Robertson, G. Amaratunga, W. Milne, J. Koskinen, Phys. Rev. B 48 (1993) 4777.
- [176] A. Lakatos, M. Abkowitz, Phys. Rev. B 3 (1971) 1791.
- [177] D. Kim, F. Merget, M. Laurenzis, P. Bolivar, H. Kurz, J. Appl. Phys. 97 (2005) 83538.
- [178] J. Kim, M. Hwang, Y. Kim, H. Kim, Y. Lee, J. Appl. Phys. 90 (2001) 2469.
- [179] K. Karch, P. Pavone, W. Windl, O. Schutt, D. Strauch, Phys. Rev. B 50 (1994) 17054.
- [180] A. Feltz, H. Aust, A. Blayer, J. Non-Cryst. Solids 55 (1983) 179.
- [181] L. Zambov, K. Weidner, V. Shamamian, R. Camilletti, U. Pernisz, M. Loboda, G. Cerny, J. Vac. Sci. Technol. A 24 (2006) 1706.
- [182] V. Rouessac, L. Favennec, B. Remiat, V. Jousseau, G. Passemard, J. Durand, Microelectron. Eng. 82 (2005) 333.
- [183] B. Wei, Y. Cheng, F. Lu, T. Chiu, H. Shih, J. Vac. Sci. Technol. A 29 (2011) 41507.
- [184] G. Dubois, W. Volksen, T. Magbitang, R. Miller, D. Gage, R. Dauskardt, Adv. Mater. 19 (2007) 3989.
- [185] W. Volksen, T. Magbitang, R. Miller, S. Purushothaman, S. Cohen, H. Nakagawa, Y. Nobe, T. Kokubo, G. Dubois, J. Electrochem. Soc. 158 (2011) G155.
- [186] D. Maidenberg, W. Volksen, R. Miller, R. Dauskardt, Nat. Mater. 3 (2004) 464.
- [187] G. Dubois, W. Volksen, T. Magbitang, M. Sherwood, R. Miller, D. Gage, R. Dauskardt, J. Sol-Gel Sci. Technol. 48 (2008) 187.
- [188] G. Ribes, J. Mitard, M. Denais, S. Bruyere, F. Monsieur, C. Parthasarathy, E. Vincent, G. Ghibaudo, IEEE Trans. Device Mater. Reliab. 5 (2005) 5.